The Pennsylvania State University

The Graduate School

College of Engineering

STRUCTURAL CHARACTERIZATION OF THE ACTIVE LAYER IN ORGANIC SOLAR CELLS

A Thesis in

Chemical Engineering

by

Derek R. Kozub

Submitted in Partial Fulfillment
of the Requirements
for the Degree of

Master of Science

August 2011

The thesis of Derek R. Kozub was reviewed and approved* by the following:

Enrique D. Gomez
Assistant Professor of Chemical Engineering
Thesis Advisor

Janna Maranas
Associate Professor of Chemical Engineering

Michael J. Janik
Assistant Professor of Chemical Engineering

Andrew L. Zydney
Head of the Department of Chemical Engineering
Walter L. Robb Chair and Professor of Chemical Engineering

*Signatures are on file in the Graduate School

ABSTRACT

Organic solar cells belong to a class of devices where the morphology of the active layer has a large impact on device performance. However, characterization of the morphology of organic semiconductor mixtures remains a challenge. We have utilized Grazing-Incidence Small-Angle X-Ray Scattering (GISAXS) and Energy Filtered Transmission Electron Microscopy (EFTEM) to characterize the morphology of polythiophene:fullerene mixtures as a function of processing conditions. GISAXS has been used to determine the domain spacing within the active layer, whereas EFTEM has been used to generate images with high contrast between domains. We have applied these methods to two promising polythiophene:fullerene systems, 1:1 mixtures of poly(3-hexylthiophene-2,5-diyl) (P3HT) and [6,6]-phenyl-C_{61} butyric acid methyl ester (PCBM) and 1:4 mixtures of poly(2,5-bis(3-tetradecylthiophen-2-yl)thieno[3,2-b]thiophene (PBTTT) and $PC_{71}BM$. In 1:1 P3HT:PCBM systems, domain compositions are found via EFTEM analysis, which are used in conjunction with DSC experiments to develop a theory for the mechanism of structural formation in polythiophene:fullerene blends. Previously, it was thought that P3HT and PCBM were immiscible, but we show that a significant amount of the non-crystallized polymer forms a mixed amorphous phase with PCBM. In 1:4 PBTTT/$PC_{71}BM$ mixtures, we show how larger domains form at long annealing times, which leads to poor performance in solar cell devices. Using the fact that large domains lead to poor performance as a guiding principle, quantitative structure-function relationships are explored for the 1:4 PBTTT/$PC_{71}BM$ and 1:1 P3HT/PCBM mixtures based on GISAXS results. Furthermore, EFTEM and GISAXS have been useful in guiding our attempts to perturb the structure of the active layer in organic solar cells. Preliminary results show that the electric field alignment of crystalline P3HT fibers in an amorphous P3HT/PCBM matrix is promising. Finally, we have discussed the limitations of EFTEM as it is currently used and how it can be expanded upon using a Focused Ion Beam (FIB) to study cross sections of solar cells.

Table of Contents

List of Figures

List of Tables

Acknowledgements

I would like to thank my advisor, Dr. Enrique Gomez, for his brilliant ideas, scientific guidance, and leadership. My scientific growth, especially in experimental work, has been greatly accelerated over the past couple of years due to his support. Through his guidance, I have learned many advanced characterization techniques, deepened my understanding of thermodynamics and polymers, and have grown in leadership. He always had the knowledge and the will that is necessary to solve problems in a difficult field. I will always remember his approach to problem solving when working on difficult problems in the future. I also want to thank him for listening and for taking my ideas into serious consideration.

I would like to thank my colleague and good friend, Kiarash Vakhshouri, for all of the hard work he put in to help me with scattering trips and TEM work. I would also like to thank him for the advice and guidance he has given me to help create new ideas.

Thank you to all members of the Gomez group. This group has originated many brilliant ideas and has done excellent experimental work that has great value to the organic solar cell community. I have great faith that this group will continue to grow and impact the cutting edge of science. It has been a pleasure working with all of you.

Thank you to the scientists at beamline 7.3.3 at the Advanced Light Source at LBNL, especially Eric Schaible and Stephen Alvarez, for their timely technical support, often during late hours of the night.

Thank you to Trevor Clark, Josh Maier, and Joe Kulik for their training and support when I was attempting difficult TEM and FIB techniques.

Thank you to my mother and father for always supporting me in my education. They encouraged me to pursue a career in science and have always done their best to raise me as a productive and responsible person. Thank you to my older brother and younger sister for being positive influences in my life. Finally, a special thank you goes to Erin Carr for her unwavering support and faith during these past few years.

Chapter 1: Introduction

Section 1.1: Motivation and Objectives

The discovery of organic semiconducting materials has created many opportunities to produce electronic devices at a potentially lower cost, one of which is the organic solar cell.[9-11] Organic solar cells are a zero-emissions alternative for electricity generation and have a promising future with device efficiencies increasing steadily over the past 10 years.[1] As shown in Figure 1 – 1, photovoltaic energy production is currently dominated by inorganic solar cells, which have a world record efficiency of 42.8% (University of Delaware)[12], much higher than the organic solar cell record efficiency of 8.3% (Konarka). However, inorganic solar cells have high energy production costs ($0.38 per kWH, assuming a 20 year lifespan) when compared to energy derived from coal ($0.006 per kWH), making them more difficult to commercialize.[13] The cost of solar energy must be reduced dramatically in order to compete with the combustion of hydrocarbons and organic solar cells are an ideal candidate to meet this goal.[9-11] The semiconducting materials in the active layer of organic solar cells are soluble in various organic solvents, so applying the active layer is similar to printing and drying an ink, rather than processing high purity semiconductor substrates, which can be very energy intensive.[9-11] Another great advantage of organic solar cells is that they can function as flexible films, which can be attached to essentially any smooth surface, regardless of the curvature.[14] Therefore, organic solar cells have the potential to compete in the same market as inorganic solar cells, but also may be used in new applications, such as supplying energy for small devices. Organic solar cells also function well when incident light is angled[15], which allows for simple applications that

do not involve solar tracking technology.

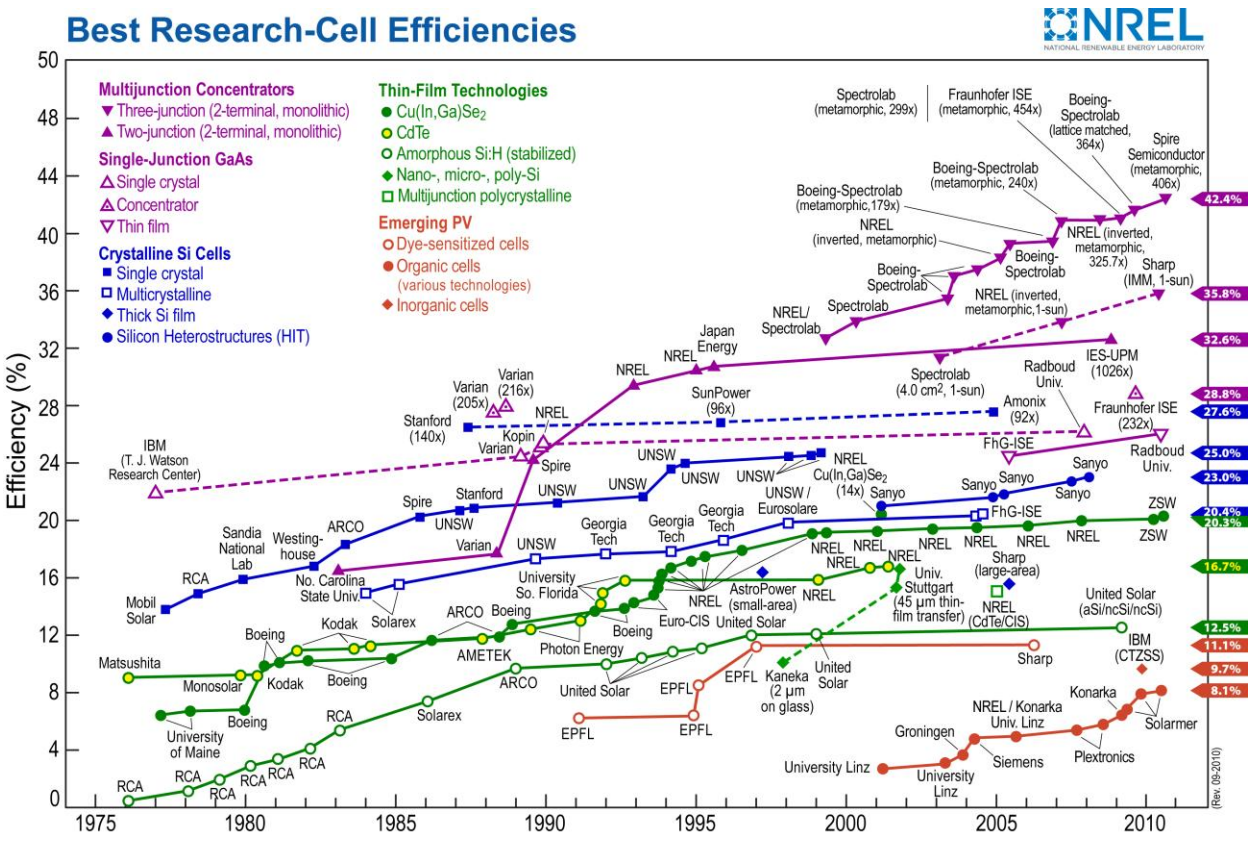

Figure 1 – 1: Record solar cell efficiencies in research laboratories vs. year of design. Research efforts in the field of organic solar cells started gaining momentum approximately ten years ago, making it one of the newest photovoltaic technologies. While efficiencies are low compared to inorganic solar cells, organic solar cells offer major advantages such as inexpensive production methods, ability to function as flexible substrates, and better functionality for applications with angled light.[1]

Optimizing the efficiency of an organic solar cell is a difficult problem because two materials, a polymer and a fullerene, are blended together to make up the active layer. The resultant morphology of this semi-crystalline blend is complex but has a strong effect on device performance. Thus, one way to approach the optimization of these devices is to study the morphology of the active layer, particularly in how it evolves at different processing conditions.[2,9-11,16-20] In this thesis, we will outline the characterization methods that can be used to quantitatively and qualitatively describe the structure of the active layer in organic solar cells,

introduce a mechanism for how the structure of the active layer forms in polythiophene/fullerene blends, comment on the role of morphology in recently developed polymer/fullerene mixtures, and provide novel ideas for characterization and morphology control of the active layer in organic solar cells.

Section 1.2: Background

Section 1.2.1: The Photoconversion Mechanism of polymer/fullerene solar cells

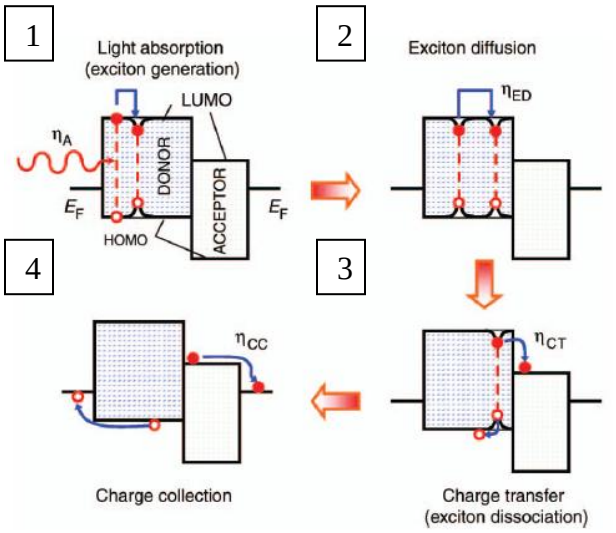

Figure 1 – 2: Photoconversion mechanism of polymer/fullerene solar cells. The polymer is referred to as a "donor" molecule and the fullerene is referred to as the "acceptor" molecule. The conductive polymer will absorb a photon, which promotes an electron from a valence band to a conducting band, forming an exciton pair. The exciton pair must diffuse through the polymer domain to the interface between the two materials where the exciton splits. The electron is donated to the fullerene domain and the hole remains in the polymer domain. The work functions of each material make it favorable for the electron to go from the conducting band of the polymer to the conducting band of the fullerene ($E_{CB,donor} > E_{CB,acceptor} > E_{VB,donor}$) instead of recombining in the polymer domain. Once the charges have separated, they must diffuse in opposite directions through their respective domains for charge collection. If enough of these events occur, an electric current will be generated. [21]

Optimizing the efficiency of each step in the conversion mechanism should create a higher electric current, but preventing the exciton pairs from recombining can be difficult. The first step in Figure 1 – 2 involves the promotion of an electron from the highest occupied molecular orbital (HOMO) level to the lowest unoccupied molecular orbital (LUMO) level in the polymer. Visible light absorbance will dictate the number of electron-hole pairs (excitons) that can be generated at varying wavelengths of solar radiation and is mostly material dependent. However, exciton diffusion within the polymer domain (step 2) is strongly affected by the morphology of the active layer. Excitons have a limited diffusion length that is on the order of 10 nm so smaller domains are preferred.[22-25] The crystallinity of the polymer domains also plays an important role in this step. Highly ordered crystalline domains are preferred because they have overlapping π-orbitals that will allow charge transfer in more directions.[26] In step 3, a large interfacial area between domains is thought to be preferred because it will reduce the exciton concentration at the polymer-fullerene interface. In step 4, charge transfer can depend on the purity of each phase. Any phase that is not pure will have adjusted electron/hole mobility characteristics, and thus will affect the performance of the device. The domains should also be interconnected to allow a route to the charge collection interfaces. Isolated domains will not contribute to the overall efficiency of the device.[21]

Section 1.2.2: Current methods and challenges of characterizing the structure of the active layer in organic solar cells

Characterization of the phase separation in organic semiconductor mixtures has been a strong focus of recent work.[2,17-19,27-33] In devices made from poly(3-hexylthiophene-2,5-diyl) (P3HT) and [6,6]-phenyl-C_{61} butyric acid methyl ester (PCBM), direct imaging of the composite films has been attempted through atomic force microscopy (AFM)[16,17,19] and transmission

electron microscopy (TEM).[2,17,19,31] P3HT and PCBM are primarily comprised of carbon and do not contain atoms with a significantly high atomic scattering factor.[34] Thus, contrast is inherently weak between domains in TEM images and the origin of contrast is not clear in either TEM or AFM. Furthermore, AFM is a surface-sensitive technique, and recent work has shown that P3HT selectively wets the air surface of P3HT:PCBM films.[35,36] Morphological characterization of semiconductor mixtures utilized in organic photovoltaics remains a challenge, and consequently, the factors governing structural evolution remain poorly understood.

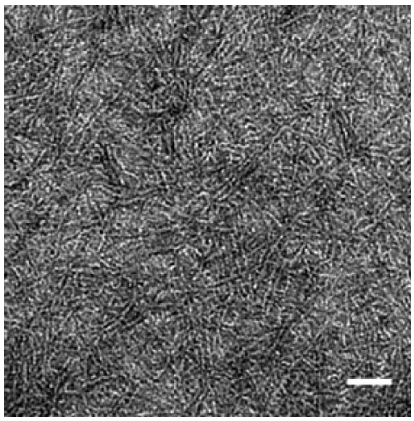

Figure 1 – 3: Bright Field Image of a 1:1 P3HT:PCBM film annealed at 130 °C for 20 min from van Bavel et al.[2] Scale bar: 200 nm

There have been numerous reports in the literature of defocusing TEM images of P3HT:PCBM mixtures in an effort to create contrast between domains.[17,31] Defocusing a TEM changes the transfer function of the microscope and limits its resolution. If enough defocus is used, the oscillating portion of the transfer function may have influence on the length scale of interest, giving large intensity fluctuations in the image and the appearance of structure.[34] Defocusing is not a robust method for determining qualitative information about P3HT:PCBM mixtures and is a very poor measure of quantitative information. Despite the difficulty in creating contrast between P3HT and PCBM domains, there have been some reports of in-focus bright field TEM images of highly ordered systems taken at low magnification.[2,37] However,

contrast is weak, the origin of contrast is not clear, and this method is not applicable to less ordered systems. Figure 1 – 3 shows a bright field image of a 1:1 P3HT:PCBM mixture, where low molecular weight (M_n = 19 kg/mol) and highly regioregular (98% H-T) P3HT is used, which may be the reason that well-defined P3HT crystals exists when limited thermal annealing is applied (130 °C for 20 min).

Section 1.3: Thesis Overview

In this thesis, we present methods for determining qualitative and quantitative information about polymer/fullerene mixtures, which leads to a better understanding of device functionality and also leads to ideas for optimizing the morphology in organic solar cells. In Chapter 2, Energy Filtered Transmission Electron Microscopy (EFTEM) is presented, which gives high contrast TEM images without sacrificing resolution. EFTEM is also used to determine domain composition. Grazing-Incidence Small-Angle X-Ray Scattering (GISAXS), a method that is very useful for determining length scales within polymer/fullerene thin film mixtures is presented as well. These two methods will be applied to the classic P3HT:PCBM mixture in tandem with differential scanning calorimetry (DSC) to create a theory for structural evolution in polythiophene/fullerene blends.

In Chapter 3, EFTEM and GISAXS will also be used to describe the phase separation that occurs in mixtures of poly(2,5-bis(3-tetradecylthiophen-2-yl)thieno[3,2-b]thiophene (PBTTT) and $PC_{71}BM$, which is thought to co-crystallize upon thermal annealing. PBTTT/$PC_{71}BM$ structural data will be related to solar cell device performance.

In Chapter 4, we will show how GISAXS length scales are related to device efficiency in P3HT:PCBM bulk heterojunction solar cells. A study on the importance of morphology recently developed polymer/fullerene mixtures is presented as well. Finally, ideas on how to improve characterization and morphology control of the active layer in organic solar cells will be presented.

Chapter 2: The formation of mesoscale structure in polythiophene/fullerene blends

Section 2.1: Overview

Here, we report the use of Energy Filtered Transmission Electron Microscopy (EFTEM) to generate high contrast images of the morphology in polythiophene/fullerene mixtures. Further, elemental maps depict the local elemental composition of the domains. In conjunction with complementary data from Grazing-Incidence Small-Angle X-Ray Scattering (GISAXS), EFTEM images allow us to examine the morphology evolution. Our approach, widely applicable to many organic semiconductor mixtures, enables characterization of the phase separation and morphology in thin films with varying degrees of long-range order.

We demonstrate that a significant amount of un-crystallized polymer exists as a homogeneous polythiophene/fullerene mixture among rod-like polythiophene crystals. Elemental analysis of the amorphous regions demonstrates partial miscibility of P3HT and PCBM. By determining the interaction parameter, χ, and the Flory-Huggins phase diagram, we predict miscibility for P3HT volume fractions greater than 0.42. We find miscibility to suppress fullerene crystallization. The combination of miscibility and suppression of fullerene crystallization at compositions near the optimum for solar cells (~0.6 volume fraction P3HT)[2,30,32] suggests that the nanoscale morphology, and consequently the device performance, is driven by polymer crystallization from partially miscible blends.

Section 2.2: Experimental Methods

Solutions of regioregular P3HT (96% H-T regioregular, M_n = 28 kg/mol, polydispersity = 1.9, Merck), regiorandom P3HT (M_n = 30 kg/mol, polydispersity = 3, Sigma-Aldrich) and

PCBM (>99.5%, Nano-C) were made with anhydrous chlorobenzene (Sigma-Aldrich) in a N_2 glovebox. Solutions were stirred for a minimum of 1 hr and heated to 100 °C for 10 seconds prior to use to ensure dissolution.

To simulate conditions relevant to organic solar cells, thin films of P3HT:PCBM were cast on 100 nm poly(3,4-ethylenedioxythiophene) poly(styrenesulfonate), PEDOT:PSS, (Clevios P, H.C. Starck) films deposited on silicon wafers. Silicon wafers were cleaned through sonication for 10 min in acetone and isopropanol followed by 10 min of UV-ozone treatment. Thin films (ca. 70 ± 10 nm) for TEM experiments were made by spin coating 15 mg/mL P3HT:PCBM solutions in a N_2 glove box at 1000 rpm for 1 min. Films were floated-off in distilled water and picked up with copper TEM grids. Samples were dried for 24 hrs under vacuum and subsequently annealed on a calibrated digital hot plate in a N_2 glove box. Films were rapidly cooled to room temperature after annealing was complete by placing them on a metal surface.

TEM experiments took place at the National Center for Electron Microscopy, Lawrence Berkeley National Laboratory on a Zeiss LIBRA 200MC. Bright field images, thickness maps and elemental maps were captured. Sulfur and carbon elemental maps were obtained through the standard three-window method.[38]

Grazing-Incidence Small-Angle X-Ray Scattering (GISAXS) experiments were conducted on beam line 7.3.3 at the Advanced Light Source, Lawrence Berkeley National Laboratory (λ = 1.24 Å). In a similar manner as for TEM samples, P3HT:PCBM thin films (ca. 152 ± 11 nm) were spun-cast on PEDOT:PSS/silicon substrates from 24 mg/mL solutions. Samples were annealed on the PEDOT:PSS/silicon substrate inside the N_2 glove box. GISAXS data was taken at angles above the critical angle for P3HT (0.135°) but below the silicon critical

angle (0.21°)[39]. In-plane data was corrected for scattering from air and the substrate as described in Section 2.3.2.

Samples for Differential Scanning Calorimetry experiments (Q1000, TA Instruments) were made by mixing P3HT and PCBM together at various concentrations. Scans were performed from 40 ^{o}C to 300 ^{o}C at 5 ^{o}C/min.

Section 2.3: Structural Characterization of P3HT/PCBM Mixtures

Section 2.3.1: Energy Filtered Transmission Electron Microscopy

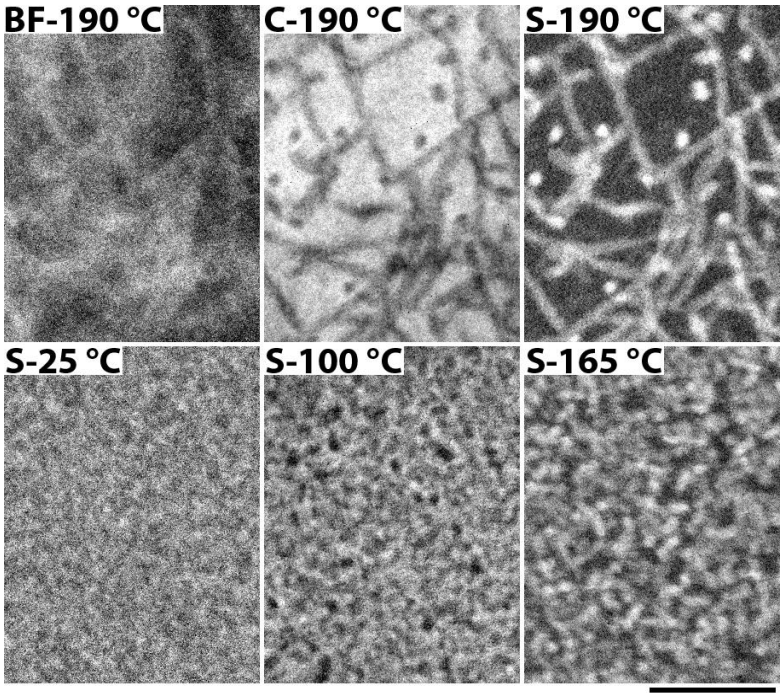

Figure 2 -1: Top: Bright field (BF), carbon map (C), and sulfur map (S) for a 1:1 P3HT/PCBM film annealed for 30 min. The same region of the sample is shown and images were taken at zero defocus. Bottom: Sulfur maps of 1:1 P3HT/PCBM films annealed at 25 °C, 100 °C, and 165 °C. The image intensities of sulfur maps are proportional to the sulfur concentration and the light regions correspond to P3HT-rich domains. Unannealed films (25 ^{o}C) show little structure, while films annealed at high temperatures, such as 190 ^{o}C, exhibit the presence of P3HT fibers in a PCBM-rich matrix. Scale bar: 200 nm.

Although P3HT:PCBM mixtures have been intensively studied,[2,3,11,31,33,36,40-49] the extent of miscibility and the domain composition remain unknown. By taking advantage of inelastic losses due to electron-sample interactions in the electron microscope, EFTEM allows for mapping of the local elemental composition through the standard three-window method.[38] The active layers of polythiophene/fullerene solar cells are ideal candidates for elemental mapping due to the large differences in sulfur and carbon densities between P3HT and PCBM. Indeed, the sulfur and carbon elemental maps show more contrast than the bright field image in Figure 2 – 1. The intensity of the elemental maps is directly proportional to the elemental concentration within domains.[38] The rod-like P3HT crystallites are clearly visible in the elemental maps as light and dark regions in the sulfur and carbon maps, respectively.

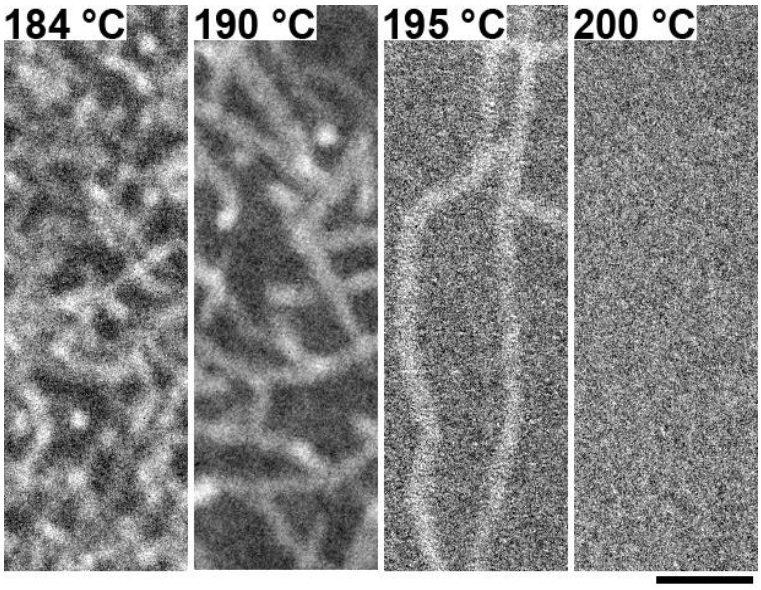

Figure 2 – 2: The structural evolution of 1:1 P3HT/PCBM mixtures as the annealing temperature approches the melting point of P3HT. All films were annealed for 30 min. Fiber diameter and length increases with higher annealing temperature, whereas the volume fraction of pure crystalline P3HT decreases with higher annealing temperatures. Scale bar: 100 nm.

Elemental mapping is a powerful technique for examining the structural evolution in polythiophene/fullerene mixtures, as shown in the bottom panel of Figure 2 – 1. As cast films show little structure, while P3HT fibers are clearly visible for films annealed at 165 and 190 ^{o}C. Although increasing the annealing temperature increases the fiber length and fiber diameter, the concentration of fibers also decreases, as shown in Figure 2 – 2. The presence of fiber-like P3HT crystals throughout P3HT:PCBM mixtures suggests that the P3HT crystallization dominates the mesostructure formation process. Furthermore, annealing films at 200 ^{o}C leads to films with no mesoscopic structure. Thus, the EFTEM results suggest that P3HT and PCBM are miscible.

Given that sulfur is only present in P3HT, the local concentration of P3HT can be found by

$$\phi_{P3HT}(x,y) = \frac{\bar{\phi}_{P3HT}}{\bar{I}} \frac{t(x,y)}{\bar{t}} I(x,y) \tag{1}$$

where $\phi_{P3HT}(x,y)$ is the local volume fraction of P3HT, $\bar{\phi}_{P3HT}$ is the average concentration of P3HT, $\bar{I}$ is the intensity averaged over the entire image, *t(x,y)* is the local sample thickness, $\bar{t}$ is the average thickness of the sample, and *I(x,y)* is the local intensity of the elemental map. Since TEM images are 2-D projections of the structure, $\phi_{P3HT}(x,y)$ is integrated over the entire sample thickness. In Figure 2 – 2, various regions exist where either no P3HT fibers are present or only one fiber is present. Thus, we can use equation 1 to compute the domain compositions of P3HT:PCBM films. $\bar{\phi}_{P3HT}$ is taken to be the composition in solution prior to spin-coating; this has been verified in previous works by measuring the fluorescence-yield of Near Edge X-ray

Absorption Fine Structure experiments.[35,50] $t(x,y)$ and $\bar{t}$ are obtained from thickness maps taken from the same region as the elemental maps. After averaging results over 6 regions in 4 images in 1:1 P3HT/PCBM systems annealed at 190 °C for 30 min, we find that ϕ_{P3HT} is 0.45 ±0.04 for the PCBM-rich domains and ϕ_{P3HT} is 0.99 ±0.08 for the center of the P3HT fibers (assuming cylindrical fibers in a PCBM-rich matrix) for films annealed at 190 ^{o}C for 30 min. We can confirm our estimate of the domain composition by independently computing the volume fraction of fibers visible in Figure 2 – 2. We find that the volume fraction of P3HT which forms fibers is 0.23 ±0.02 for films annealed at 190 °C for 30 min. Thus, given that $\bar{\phi}_{P3HT}$ is 0.58 we can estimate that ϕ_{P3HT} in the PCBM-rich domains is 0.45 ±0.02, in excellent agreement with our results obtained from equation 1.

Section 2.3.2: Grazing-Incidence Small-Angle X-Ray Scattering Data Reduction

In this work, we focus on the in-plane data at the specular reflection and assume the Born Approximation is valid. Detector dark counts and empty-cell scattering are subtracted and data is normalized by the incident scattering intensity and the intensity of the scattered beam. Since our samples are composed of P3HT:PCBM films on top of PEDOT:PSS we model our films as being composed of two distinct layers. If the critical angle of the underlying layer (layer 1) is less than or equal to the critical angle of the top layer (layer 2), then the in-plane scattered intensity of the top layer, I_2, is given by

$$I_2 = I_{1+2} - c_A(\alpha_i)\, c_B(\alpha_i)\, I_1 \qquad (2)$$

where I_{1+2} is the total GISAXS intensity, I_1 is the scattering from the PEDOT:PSS film on Si, α_i is the angle of incidence, and $c_A(\alpha_i)$, $c_B(\alpha_i)$ are constants which depend on the incident angle. $c_A(\alpha_i)$ accounts for the variation in scattering volume as a function of X-ray penetration depth into the film, $\Lambda(\alpha_i)$, and is given by:

$$c_A(\alpha_i) = \left(\frac{\Lambda(\alpha_i) - t_2}{\Lambda(\alpha_i)} \right) \tag{3}$$

where

$$\Lambda(\alpha_i) = t_1 + t_2 \tag{4}$$

if

$$\Lambda(\alpha_i) \geq t_1 + t_2 \tag{5}$$

t_2 is the thickness of the top film (layer 2, P3HT:PCBM in our case) and t_1 is the thickness of the first layer (PEDOT:PSS). $\Lambda(\alpha_i)$ is constrained to be less than $t_1 + t_2$ since the incident angles used in this work are larger than the critical angle of the P3HT:PCBM film (0.135^o) but less than the critical angle of silicon (0.21^o).[39] Thus, our scattering geometry prevents X-rays from penetrating into the Si substrate. $c_B(\alpha_i)$ in equation 6 accounts for the exponential decay of the intensity as a function of film depth:

$$c_B(\alpha_i) = \frac{1 - e^{-\left(\frac{\Lambda(\alpha_i) - t_2}{\Lambda(\alpha_i)}\right)}}{1 - e^{-1}} \tag{6}$$

where now if $\Lambda(\alpha_i) \leq t_2$, $c_B(\alpha_i) = 0$, since the X-ray intensity decays to zero before reaching the underlying film (layer 1). The penetration depth, Λ, is given by:[51]

$$\frac{1}{\Lambda(\alpha_i)} = -2k_0 \, \mathrm{Im}\left[\sqrt{\alpha_i^2 - \alpha_c^2 - 2i\beta}\right] \tag{7}$$

k_0 is $2\pi/\lambda$, α_c is the critical angle, and β is $\lambda\mu/4\pi$ (μ is the linear absorption coefficient). α_c and β for P3HT:PCBM films were calculated through standard methods.[51]

As an example of our procedure, Figure 2 – 3a shows the in-plane GISAXS intensity versus scattering vector for a P3HT:PCBM film annealed at 190 °C for 30 min which was cast on PEDOT:PSS/silicon and for PEDOT:PSS cast on silicon. Figure 2 – 3b shows the data after subtraction of the substrate scattering. Note that the scattering from the substrate is a small contribution to the total intensity from P3HT:PCBM films cast on PEDOT:PSS/silicon.

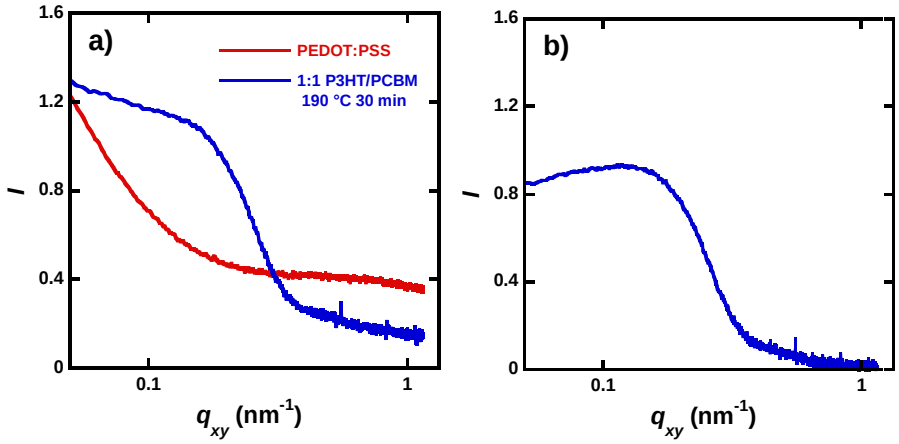

Figure 2 – 3: a) Raw GISAXS intensity *vs.* scattering vector for a PEDOT:PSS film and 1:1 P3HT:PCBM film on top of a PEDOT:PSS film annealed at 190 °C for 30 min. b) Scattering curve for 1:1 P3HT:PCBM film annealed at 190 °C for 30 min after subtraction of the substrate scattering.

Section 2.3.3: Grazing-Incidence Small-Angle X-Ray Scattering Results

We can complement and confirm our measurements of morphological evolution in polythiophene/fullerene mixtures through GISAXS. Grazing-incidence X-ray scattering has been demonstrated to be a powerful technique for studying polymer thin films.[3,18,46,52-54] In GISAXS, the scattering is acquired in the reflection geometry with incident angles near the critical angle of the film to minimize the contribution of the substrate to the scattering intensities.[51,52] With this technique, a quantitative measure of the mesostructure in organic semiconductor mixtures can be obtained.

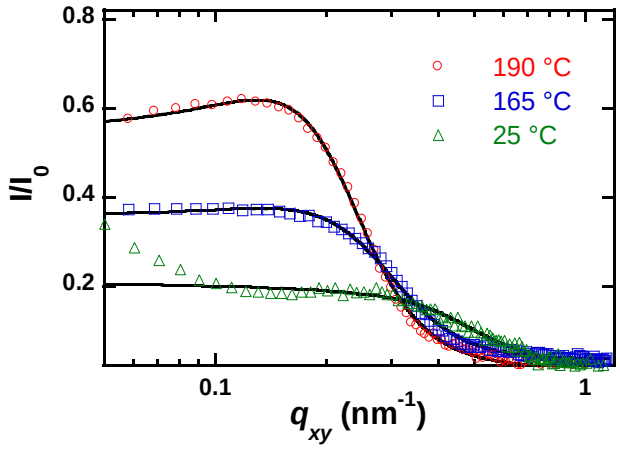

Figure 2 – 4: GISAXS intensity vs. scattering vector, *q*, for 1:1 P3HT:PCBM mixtures annealed at various temperatures for 30 min. The solid lines are Teubner-Strey fits to the data.

Figure 2 – 4 shows the GISAXS intensity as a function of the in-plane scattering vector, q_{xy}, for films annealed at various temperatures for 30 min. Consistent with the sulfur elemental map shown in Figure 2 – 1, little structure is apparent after the film is cast prior to thermal annealing. This suggests that the film-casting process briefly plasticizes the film and allows for limited crystallization of P3HT to occur.[3] Annealing leads to the formation of structure, as evident in the increase in the scattering intensity at low *q* after thermal annealing. The intensities, however, approach a finite value as *q* approaches zero, suggesting little macroscale phase separation is present after annealing.

Extracting structural parameters of the morphology from GISAXS intensities requires fitting to a model. The morphologies visible in Figure 2 – 1 are poorly ordered yet possess a characteristic length scale corresponding to the P3HT crystal dimension; visually, they resemble polymer microemulsions.[55] As shown by the solid curves in Figure 2 – 4, the use of the Teubner-Strey scattering function, originally developed for oil/water/microemulsions[56] and later extended to polymer blends,[57,58] describes the GISAXS data well over a wide *q*-range for

samples annealed at elevated temperatures. The upturn in the intensities at low-q of the scattering data from as-cast films prior to thermal annealing is not captured by Teubner-Strey and is most likely due to macrophase separation or structures larger than 150 nm. Thus, we assume that Teubner-Strey is an appropriate model for describing the mesostructure visible in Figure 2 – 1 for unannealed P3HT:PCBM films. Figure 2 – 4 demonstrates that Teubner-Strey is an appropriate model for describing scattering from P3HT:PCBM films.

In order to quantify the structure in polythiophene/fullerene mixtures, we fit the Teubner-Strey (T-S) scattering function to the GISAXS data. T-S was originally developed for bicontinuous microemulsions and is given by:[56]

$$I(q) = \frac{1}{a_2 + c_1 q^2 + c_2 q^4} + I_{bgd}(q) \tag{8}$$

where a_2, c_1, and c_2 are fitting parameters, q is the scattering vector, and $I_{\text{bgd}}(q)$ is a background function employed in polymeric systems. $I_{\text{bgd}}(q)$ is speculated to account for the connectivity of polymer chains and is assumed to be of the form $I_{\text{bgd}}(q) = (eq^2+f)^{-1}$, where e and f are fitting constants. [57,58] Fitting the GISAXS data to T-S yields the domain periodicity, d, correlation length, $\xi_{TS,}$ and the amphiphilicity factor, f, through:

$$d = 2\pi\left[\frac{1}{2}\left(\frac{a_2}{c_2}\right)^{1/2} - \frac{1}{4}\frac{c_1}{c_2}\right]^{-1/2} \tag{9}$$

$$\xi_{TS} = \left[\frac{1}{2} \left(\frac{a_2}{c_2} \right)^{1/2} + \frac{1}{4} \frac{c_1}{c_2} \right]^{-1/2} \tag{10}$$

$$f = \frac{c_1}{\sqrt{4 a_2 c_2}} \tag{11}$$

since T-S is consistent with a real-space pair-correlation function, *g(r)*, given by:

$$g(r) = \frac{d}{2\pi r} \exp\left[-r / \xi_{TS} \right] \sin\left(\frac{2\pi r}{d} \right) \tag{12}$$

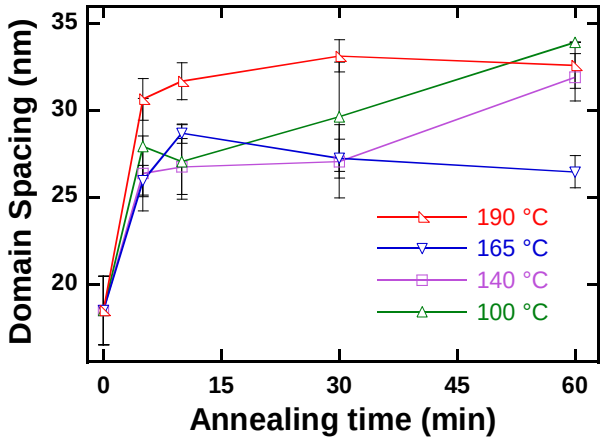

Figure 2 – 5: Domain spacings from GISAXS data of 1:1 P3HT:PCBM mixtures at various annealing conditions. Note that films annealed at 165 ^{o}C and 190 ^{o}C appear to approach a steady state within the time scale of our experiments. Lines are guides to the eye. Error bars denote the standard deviation of multiple measurements.

Using Teubner-Strey as a model for the scattering data, the morphology in terms of the domain spacing, *d*, can be quantified. We examined films annealed at 100, 140, 165 and 190 ^{o}C for 5, 10, 30 and 60 min, as shown in Figure 2 – 5. At 100 and 140 ^{o}C, the domain spacing grows with time, suggesting coarsening of the structure. At 165 and 190 ^{o}C, however, *d* increases quickly and then appears to approach a steady state. The arrest of the structural evolution at elevated annealing temperatures suggests that P3HT and PCBM are miscible; further coarsening does not occur or is strongly suppressed.

Section 2.3.4: GISAXS and EFTEM Comparison

Comparison between GISAXS and EFTEM data is challenging. In order to facilitate comparisons between the two techniques, we calculated the domain size from GISAXS data and compared these values to the fiber width measured from EFTEM experiments. We find the domain size from *g(r)* by extrapolating the slope of *g(r)* from *g(r)* ~ 1 to the minimum value of *g(r)* as shown in Figure 2 – 6.[59] Sulfur and carbon maps were used to measure the diameter of

P3HT fibers. As shown in Figure 2 – 7, measurements of the domain size from GISAXS are in good agreement with the fiber width measured from elemental maps, which were analyzed by measuring the full-width half max of the scattering intensity. The domain size of 12 nm is constant with annealing temperature until 190 ^{o}C, whereupon d_c increases to approximately 17 nm.

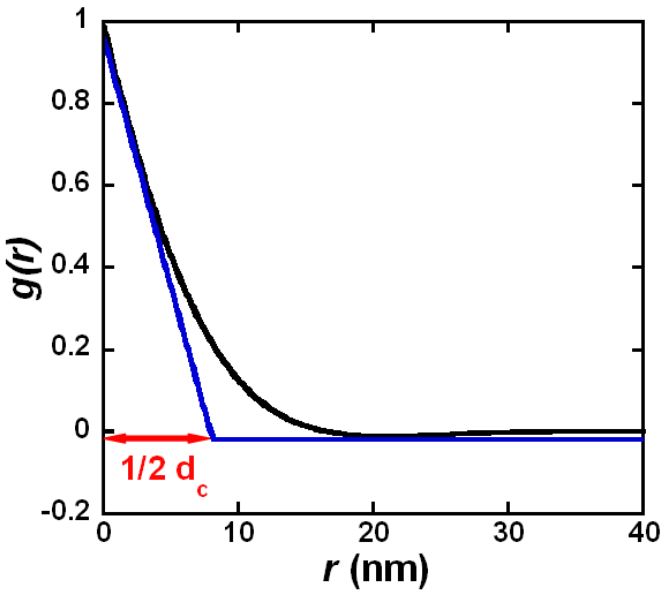

Figure 2 – 6: *g(r)* for a 1:1 P3HT:PCBM film annealed at 190 °C for 30 min. The blue lines illustrate the procedure for finding the domain size, d_c.

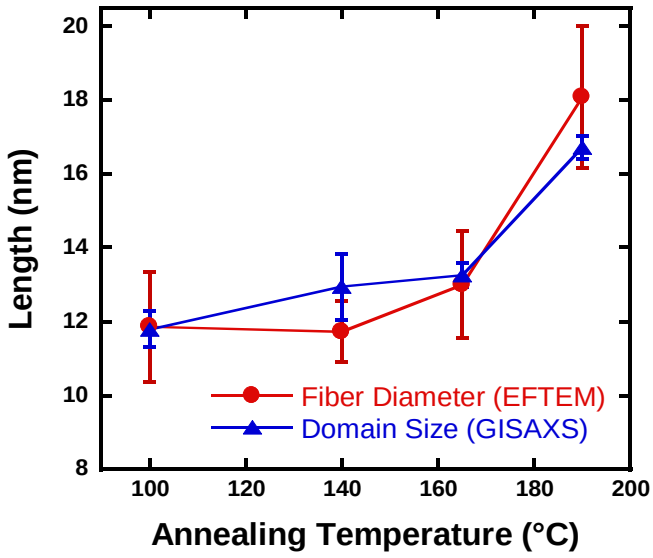

Figure 2 – 7: Domain sizes from GISAXS and fiber diameters obtained from EFTEM elemental maps for 1:1 by mass P3HT:PCBM films annealed at various temperatures for 30 min. The error bars denote the standard deviation over multiple measurements.

Section 2.3.5: The Amphiphilicity Factor

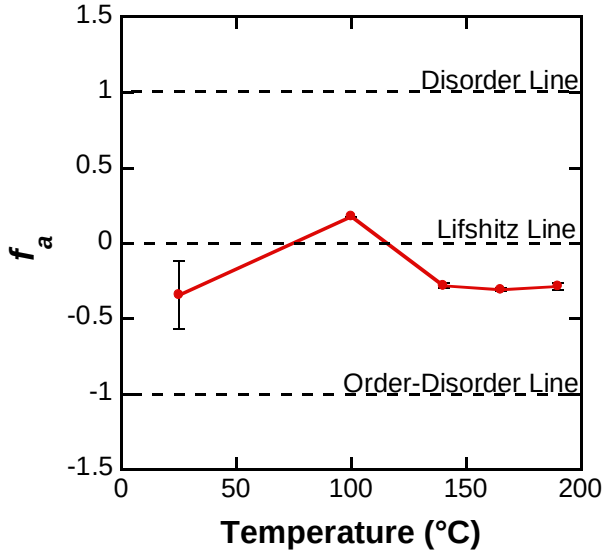

Figure 2 – 8: The amphiphilicity factor vs. temperature for 1:1 P3HT/PCBM mixtures annealed for 60 min according to the Teubner-Strey scattering model.

The amphiphilicity factor is a direct result of the Teubner-Strey analysis and measures how closely the scattering data resembles a bicontinuous microemulsion. Typically, ordered microemulsions will give an amphiphilicity factor between 0 and -1. Physically, this is represented by a vanishing surface tension between domains in the oil/water/surfactant system. The Lifshitz line, where f_a is 0, is the cutoff between what is considered to a good microemulsion ($-1 < f_a < 0$) and a poor microemulsion ($0 < f_a < 1$).[58,60,61] Although the physical interpretation of Teubner-Strey does not apply to our system, we examined the amphiphilicity factor vs. temperature for 1:1 P3HT/PCBM mixtures annealed for 60 minutes. For 25, 140, 165, and 190 °C, the amphiphilicity factor is within the range of what is considered a good microemulsion. However, at 100 °C, the amphiphilicity factor characterizes the structure as a poor microemulsion. Interestingly, the mixture at 100 °C also appears to have unique EFTEM results as well. In this system, we find that there are three phases, a pure PCBM phase, a mixed P3HT:PCBM phase, and a pure P3HT phase, which are represented by the dark, grey, and light regions of the sulfur map in Figure 2 – 1. One explanation for a poor amphiphilicity factor is that the periodic behavior of the model is interrupted, which is evident in a three phase system. Thus, the amphiphilicity factor results are in agreement with the hypothesis that three phase systems form at lower annealing temperatures and two phase systems form at higher annealing temperatures.

Section 2.4: Miscibility of P3HT/PCBM Mixtures

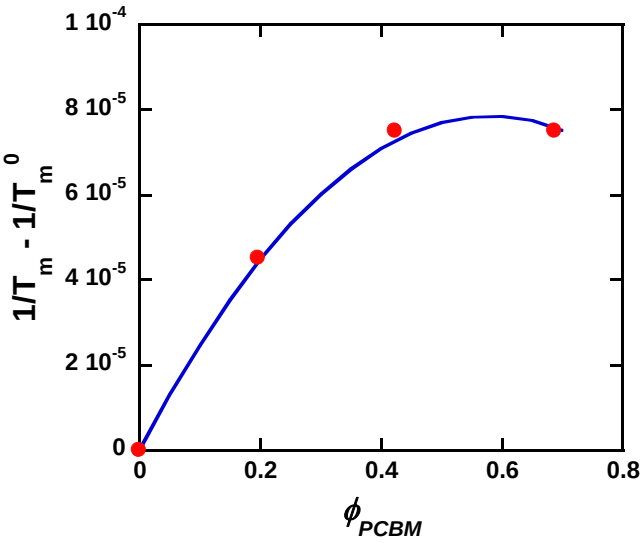

Figure 2 – 9: Estimate of the miscibility from measurements of the melting point depression. Melting point depression of P3HT as a function of PCBM volume fraction, ϕ_{PCBM}, obtained from DSC experiments. The solid line is from equation 13 with χ = 0.86.

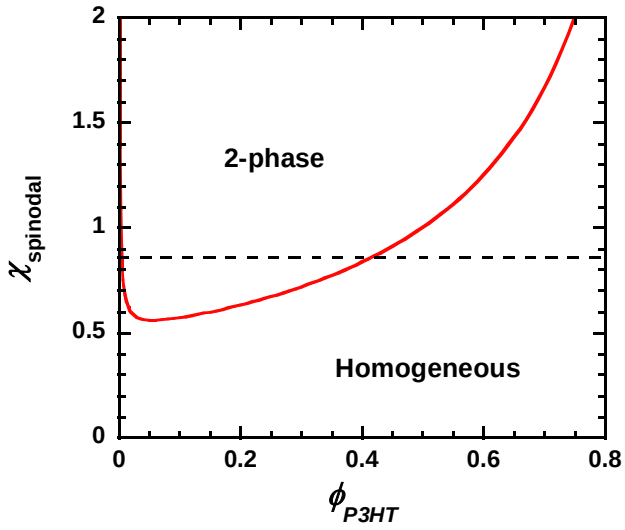

Figure 2 – 10: Spinodal as a function of P3HT volume fraction, ϕ_{P3HT}, obtained by modeling P3HT:PCBM mixtures as polymer solutions with MW_{P3HT} = 50,000 g/mol. The dotted line denotes χ = 0.86, and in combination with the spinodal indicates that homogeneous P3HT:PCBM mixtures are unstable for ϕ_{P3HT} < 0.42.

We can obtain a direct measure of the chemical interactions by measuring the melting point depression of P3HT in P3HT:PCBM mixtures. Through Differential Scanning

Calorimetry, we can obtain an estimate of the Flory-Huggins interaction parameter, χ, using equation 13:[62]

$$\frac{1}{T_m} - \frac{1}{T_m^{\,0}} = \frac{R}{\Delta H_f}\frac{v_m}{v_s}\left(\phi_s - \chi\phi_s^{\,2}\right) \tag{13}$$

where T_m is the melting point at a solvent (PCBM) volume fraction ϕ_s, $T_m^{\,0}$ is the melting point of pure polymer, R is the ideal gas constant, ΔH_f is the heat of fusion of polymer, v_m is the monomer molar volume of polymer ($v_{m,P3HT}$ = 151 cm^3/mol)[63] and v_s is the solvent molar volume ($v_{s,PCBM}$ = 607 cm^3/mol)[64]. ΔH_f is obtained from the melting endotherm. Fitting equation 13 to the melting point data shown in Figure 2 - 9 with χ as the only adjustable parameter yields χ = 0.86 +/- 0.09. The error in χ is estimated from the uncertainty of the fit. In combination with the spinodal for polymer solutions shown in Figure 2 – 10, χ allows for the determination of the miscibility of P3HT:PCBM mixtures. We find that for P3HT concentrations greater than 0.42 by volume, the mixtures are miscible. Therefore, the structure present in 1:1 by mass mixtures (ϕ_{P3HT} = 0.58) utilized in both the experiments illustrated in Figures 2 – 1, 2 – 2, 2 – 3, and 2 – 4 and in organic solar cells commonly reported in the literature[9,65] is not a result of phase separation in the polymer solution, but instead, must be a consequence of polymer crystallization.

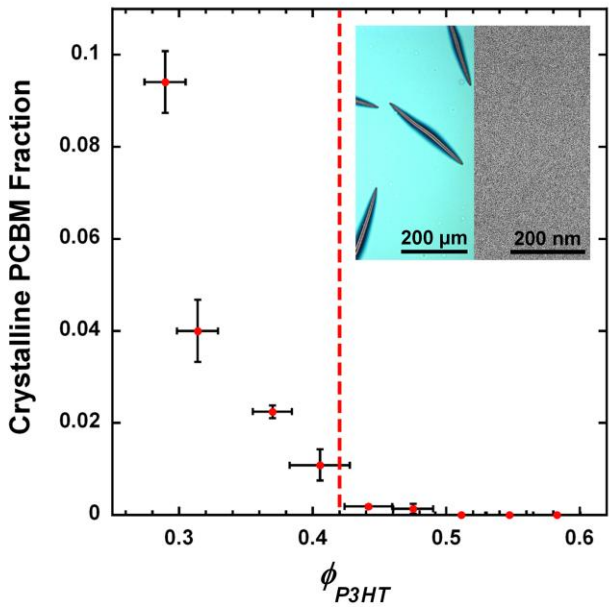

Figure 2 – 11: PCBM crystallization in regiorandom P3HT:PCBM films as a function of ϕ_{P3HT}. The dotted line corresponds to ϕ_{P3HT} = 0.42. PCBM crystallization is estimated from the area fraction of PCBM crystals visible in optical micrographs (inset, left). The film shown in the optical micrograph (ϕ_{P3HT} = 0.37) was annealed at 190 °C for 30 min. Sulfur elemental maps indicate that the films are homogeneous at nanometer length scales (inset, right). The sulfur map shown is of a regiorandom P3HT:PCBM film with ϕ_{P3HT} = 0.58 annealed at 190 °C for 30 min. Note that Figure 4 predicts P3HT:PCBM mixtures to be miscible for ϕ_{P3HT} > 0.42. Error bars denote the standard deviation of multiple measurements.

Our results suggest that the crystallization of PCBM would be suppressed in mixtures of amorphous P3HT with PCBM if ϕ_{P3HT} > 0.42. To test this hypothesis, we mixed regiorandom P3HT, which does not crystallize, with PCBM and examined the film morphology. Figure 2 – 11 shows the PCBM crystallization as the area fraction of PCBM crystals visible in optical micrographs for films with varying composition. For regiorandom P3HT concentrations above 0.42, when the mixture is miscible, no evidence of microstructure is observed through elemental mapping even after annealing for 30 min at 190 °C (inset of Figure 2 – 11). Consistent with the Flory-Huggins phase diagram shown in Figure 2 – 10, the crystallization of fullerene is strongly suppressed at ϕ_{P3HT} above 0.42.

Section 2.5: The mechanism of structure formation in P3HT/PCBM mixtures

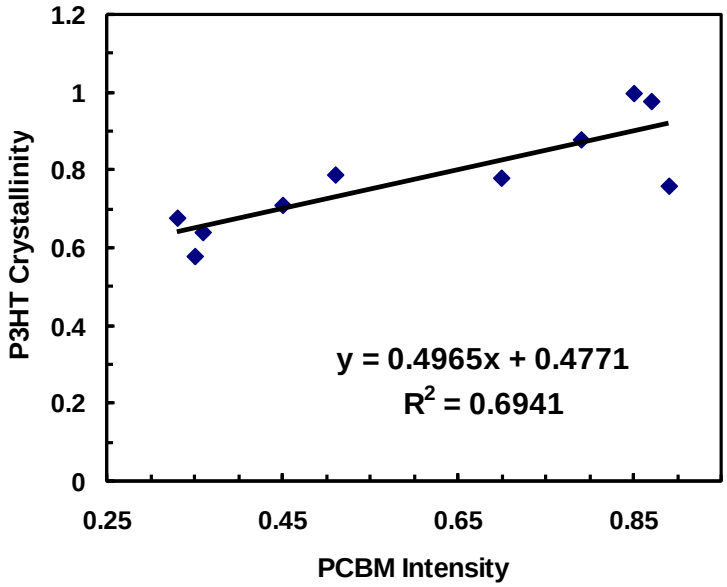

Figure 2 – 12: Grazing Incidence X-Ray Diffraction for 1:1 P3HT/PCBM mixtures.[3] The crystallinity of P3HT is plotted against the intensity of the PCBM peak for a 1:1 P3HT/PCBM mixture. PCBM intensity is proportional to crystallinity. Annealing times include 0, 5, 10, and 30 min. Data taken from "Correlating the scattered intensities of P3HT and PCBM to the current densities of polymer solar cells" by Gomez et al.

The results in Figures 2 – 1, 2 – 5, and 2 – 10 leads to the conclusion that polymer crystallization drives the structure formation process in miscible polythiophene/fullerene mixtures. As-cast films have little structure, as evident in Figures 2 – 1 and 2 – 5. Annealing enhances molecular motion and allows polythiophene to crystallize. Polymer crystallization depletes the concentration of polymer in the amorphous region, leading to macroscopic phase separation if enough polymer crystallization takes place. This conclusion is consistent with the micron-sized fullerene clusters visible through optical microscopy of 1:1 by mass P3HT:PCBM mixtures after thermal annealing,[27] the mesostructure visible in Figure 2 – 1 through EFTEM, and recent evidence from dynamic secondary ion mass spectrometry that suggests P3HT and PCBM are not completely immiscible. Thus, our results provide an explanation for the

amorphous nature of micron-sized fullerene clusters often observed in 1:1 by mass polythiophene/fullerene mixtures [3,18,53,66] – the formation of the fullerene clusters is not driven by the crystallization of fullerene, but rather by a combination of P3HT crystallization and the limited solubility of P3HT and PCBM.

The proposed mechanism for structural formation in P3HT:PCBM mixtures suggests that the crystallinity of P3HT and PCBM are correlated. When a significant amount of P3HT crystallizes, the concentration of PCBM in the amorphous domain rises. PCBM will precipitate out as a pure phase if the concentration rises above the miscibility limit. Therefore, when P3HT is removed from the amorphous phase, a similar amount of PCBM should be removed as well. The Grazing Incidence X-Ray Diffraction (GIXD) results in Figure 2 – 12 show a correlation between P3HT crystallinity and the intensity of the PCBM peak, which is proportional to PCBM crystallinity.[3] Although these results are preliminary, they suggest that the proposed mechanism for structural formation in 1:1 P3HT:PCBM mixtures is correct. Further GIXD studies will be needed to confirm this, where regioregular P3HT and regiorandom P3HT are mixed in varying proportions to control the crystallinity of P3HT in 1:1 P3HT:PCBM mixtures.

Section 2.6: Summary and Conclusions

We have shown that the intricate mesoscopic structure of polythiophene/fullerene mixtures, critical for device performance, is driven by the crystallization of the polymer. Quantifying the chemical interactions between P3HT and PCBM through the Flory-Huggins interaction parameter enables the determination of the extent of miscibility between these two components. By understanding the partial miscibility of P3HT:PCBM mixtures and knowing the volume fractions within each domain, we derive a mechanism for structure formation.

Crystallization of P3HT rejects PCBM and makes a pure P3HT phase. This process enriches the amorphous mixed phase with PCBM. If the volume fraction of PCBM rises enough, it precipitates out of the amorphous mixed phase and forms a pure PCBM phase. By providing a description of the structure formation process in polythiophene/fullerene blends, our results may lead to strategies for controlling the morphology in organic semiconductor mixtures utilized in the active layer of solar cells.

Chapter 3: Impact of Mesoscale Morphology in 1:4 poly(2,5-bis(3-tetradecylthiophen-2-yl)thieno[3,2-b]thiophene:$PC_{71}BM$ Solar Cells

Chapter 3.1: Introduction and Background

Although P3HT/PCBM solar cells have been studied extensively and work well in the bulk-heterojunction architecture (~5% efficiency), they ultimately fall short of the goal of 10% efficiency for commercialization.[11] Recent studies have shown that other polythiophenes and low band gap polymers have potential to reach higher efficiencies than are seen in the P3HT:PCBM system.[67] However, advances in chemistry must be accompanied by advances in the understanding of morphology in polymer/fullerene mixtures because both aspects must work in tandem to optimize the performance of a solar cell.[11] Therefore, it is important to study the morphology of many different types of polymer/fullerene systems. This will aid in the discovery of the universal principals that lead to better device performance. For instance, it is well established that domains on the order of 10 nm are necessary to prevent exciton recombination in organic solar cells.[22-25] However, a quantitative understanding of this phenomenon is lacking. There are also many other aspects of the morphology that need to be studied such as the compositions within each domain, the interconnectivity of crystals, interfacial area for exciton charge separation, etc. By studying a variety of polymer/fullerene systems, we can compare morphological characteristics and identify which are the most important for device performance. We have studied poly(2,5-bis(3-tetradecylthiophen-2-yl)thieno[3,2-b]thiophene (PBTTT) mixed in a 1:4 ratio with $PC_{71}BM$. The 1:4 ratio has been shown to give the highest efficiencies for the PBTTT/$PC_{71}BM$ mixture.[5,68,69]

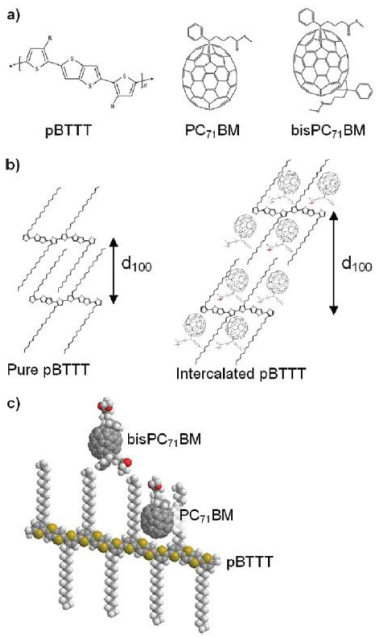

Figure 3 – 1: a) Molecular structure of PBTTT, $PC_{71}BM$, and $bisPC_{71}BM$. b) Structures thought to be present in pristine crystalline PBTTT and PBTTT:$PC_{71}BM$ mixtures. c) The extra side chain on $bisPC_{71}BM$ is thought to restrict access to the intercalation seen in PBTTT:$PC_{71}BM$ mixtures. Reproduced from "Tuning the Properties of Polymer Bulk Heterojunction Solar Cells by Adjusting Fullerene Size to Control Intercalation" by Cates et al.[5,68]

PBTTT has high potential as a conductive polymer in solar cell applications because of its high charge carrier mobility (0.2 - 0.6 $cm^2V^{-1}s^{-1}$).[68] PBTTT also has very unique properties when it is mixed with $PC_{71}BM$. Figure 3 – 1b illustrates intercalation between PBTTT and $PC_{71}BM$, which has been shown to occur via X-Ray Diffraction (XRD) experiments in 1:4 PBTTT/$PC_{71}BM$ thin films.[5,68,70] The repeating configuration is a bimolecular crystal, where PBTTT and $PC_{71}BM$ are arranged in a well-ordered stable structure. One reason for the stability of this structure is that the size of the $PC_{71}BM$ molecule is very close to the spacing between side-chains in PBTTT molecules.[68] The presence of the $PC_{71}BM$ molecule in between side chains of PBTTT prevents interdigitation between PBTTT polymer chains and thus spaces the chains further apart.[5,68] XRD is used to measure the increase in spacing and confirm the theoretical structures shown in Figure 3 – 1b. An increase in domain spacing is not observed

when PBTTT is mixed with bis$PC_{71}BM$ and Figure 3 – 1c illustrates how the side-chain on bis-$PC_{71}BM$ is too large for intercalation with PBTTT.[5]

An important motivation for studying the morphology of the active layer in polymer solar cells is the hypothesis that the structure of the active layer is related to device performance. In particular, it is hypothesized that the smaller domains are essential for creating high efficiency devices.[11] However, due to a lack of robust morphological characterization, structure-function relationships do not exist. PBTTT/$PC_{71}BM$ mixed in a 1:4 ratio is an interesting system to study because it undergoes a unique structural evolution upon thermal annealing that leads a wide range of domain sizes, making it an ideal candidate to study for structure-function relationships. We will show that increasing the size or spacing between domains decreases the device performance and is consistent with the reported exciton diffusion length of 10 nm by means of a simple model.[22-25]

Section 3.2: Experimental Methods

Solutions of poly(2,5-bis(3-tetradecylthiophen-2-yl)thieno[3,2-b]thiophene (PBTTT) (M_n = 26 kg/mol, polydispersity = 1.9, Merck) and $PC_{71}BM$ (>99.5%, Nano-C) were made with anhydrous 1,2-dichlorobenzene (Sigma-Aldrich) in a N_2 glovebox. Solutions were stirred for a several hours at 100 °C prior to use to ensure dissolution.

To simulate conditions relevant to organic solar cells, thin films of PBTTT:$PC_{71}BM$ were cast on 70 nm poly(3,4-ethylenedioxythiophene) poly(styrenesulfonate), PEDOT:PSS, (Clevios P, H.C. Starck) films deposited on silicon wafers. Silicon wafers were cleaned through sonication for 10 min in acetone and isopropanol followed by 10 min of UV-ozone treatment. Thin films (ca. 65 ± 7 nm) for TEM experiments were made by spin coating 15 mg/mL

P3HT:PCBM solutions in a N_2 glove box at 1000 rpm for 1 min. Films were floated-off in distilled water and placed on copper TEM grids. Samples were dried for 24 hrs under vacuum and annealed on a calibrated digital hot plate in a N_2 glove box. Films were rapidly cooled to room temperature after annealing was complete by placing them on a metal surface.

TEM experiments took place at the Materials Research Institute at The Pennsylvania State University on a JEOL 2010 LaB_6 and on the Zeiss Libra 200MC at The National Center for Electron Microscopy. Bright field images, thickness maps and elemental maps were captured. Sulfur and carbon elemental maps were obtained through the standard three-window method[38].

Grazing-Incidence Small-Angle X-Ray Scattering (GISAXS) experiments were conducted on beam line 7.3.3 at the Advanced Light Source, Lawrence Berkeley National Laboratory (λ = 1.24 Å). In a similar manner as for TEM samples, PBTTT/PC_{71}BM thin films (ca. 70 ± 10 nm) were spun-cast on PEDOT:PSS/silicon substrates from 24 mg/mL solutions. Samples were annealed on the PEDOT:PSS/silicon substrate inside the N_2 glove box. GISAXS data was taken at angles above the critical angle for 1:4 PBTTT/PC_{71}BM mixtures (0.135°) but below the silicon critical angle (0.21°)[39]. In-plane data was corrected for scattering from air and the substrate as described in Section 2.3.3.

Solar cells were fabricated on indium tin oxide (ITO) coated glass substrates (Kintec). The substrates were cleaned with Aquet detergent solution and water, followed by 10 min of sonication in acetone and isopropanol and 10 min of UV-ozone treatment. PEDOT:PSS was spun cast in a laminar flow hood at 4000 rpm for 2 min and subsequently dried at 165 °C for 10 min. The active layer was spun cast in a N_2 glovebox at 1000 rpm for 1 min. A 75 nm layer of aluminum was applied via thermal deposition.

Solar cell performance was tested by generating a current versus voltage curve when exposed to 1.5 AM (0.1 mW/cm^2) light from a solar simulator (Newport Model SP92250A-1000). Voltage was applied and current was measured by the Keithley 2636A Sourcemeter.

Section 3.3 Structural Characterization of 1:4 PBTTT/$PC_{71}BM$ mixtures

Section 3.3.1 Energy Filtered Transmission Electron Microscopy

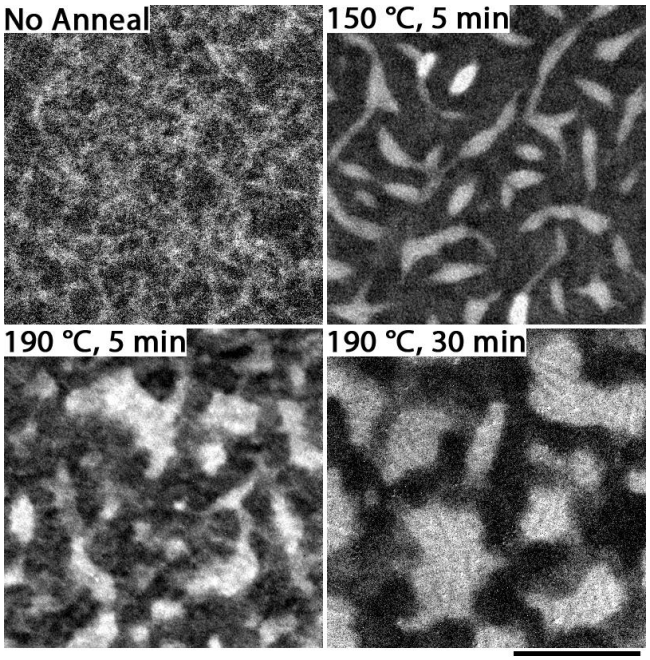

Figure 3 – 2: Sulfur Map images of 1:4 PBTTT/$PC_{71}BM$ mixtures at various annealing conditions. Pixel intensities are proportional to the concentration of sulfur, which is only present in PBTTT. The non-annealed film shows little structure whereas annealed films show larger domains with higher PBTTT purity. Scale Bar: 200 nm.

Sulfur maps of 1:4 PBTTT/$PC_{71}BM$ thin films are presented in Figure 3 – 2. In sulfur maps, bright areas correspond to regions that are rich in sulfur, which is only present in PBTTT. The non-annealed film shows little phase separation, indicating that molecular motion is limited at room temperature. Upon thermal annealing, molecular motion increases and domains that are

concentrated in PBTTT form. The sulfur maps indicate that domains concentrated with PBTTT increase in size with annealing temperature and annealing time and can range from approximately 20 – 200 nm depending on annealing conditions.

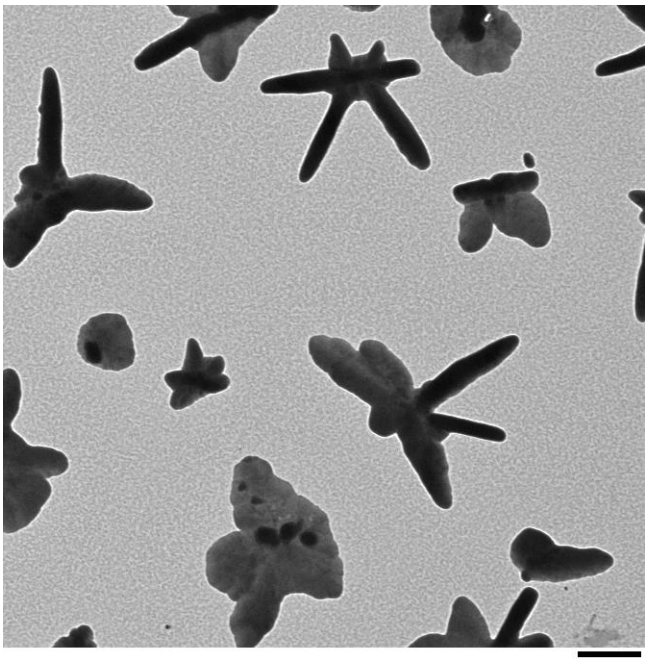

Figure 3 – 3: Bright field image of a 1:4 PBTTT/$PC_{71}BM$ film annealed for 30 minutes at 150 °C. Micron-sized $PC_{71}BM$ clusters are present in various configurations. Scale bar: 2 µm.

The structural evolution of 1:4 PBTTT/$PC_{71}BM$ films is very complex compared to the more heavily studied 1:1 P3HT/PCBM mixture for a variety of reasons. The sulfur maps in Figure 3 – 2 show that the PBTTT concentrated domains have no specific geometry and can change in size by almost and order of magnitude, whereas 1:1 P3HT/PCBM mixtures form cylindrical fibers which do not have diameters larger than 25 nm (see section 2.3.4). Also, the bright field image in Figure 3 – 3 shows the presence of micron-sized fullerene clusters in 1:4 PBTTT/$PC_{71}BM$ films annealed for 30 minutes at 150 °C. These fullerene clusters are approximately 10 times thicker than the surrounding domain. The frequency and size of $PC_{71}BM$ clusters varies greatly with annealing conditions, where longer annealing times lead to a

higher frequency and size. Furthermore, Figure 3 – 2 shows the presence of a structure within the PBTTT domains of the film annealed at 190 °C for 30 min. Interestingly, it has been reported that bimolecular crystals form between 180 – 250 °C[70], suggesting that intercalation affects the structure of the PBTTT domain on the order of 10 – 20 nm as well. One hypothesis for why this occurs is that the bimolecular crystal and the pure PBTTT crystal alternate periodically within the PBTTT domain. Thus, Figures 3 – 2 and 3 – 3 clearly depict 3 levels of structure in 1:4 PBTTT/PC71BM films: micron-sized fullerene clusters, a mesoscale structure between PBTTT and $PC_{71}BM$ domains, and an internal structure to PBTTT domains. In addition, a 4th level of structure due to intercalation has been shown to exist on the molecular level.[5,68] For this reason, the mechanism of structure formation for P3HT/PCBM mixtures found in Section 2.5 does not apply to PBTTT/$PC_{71}BM$ mixtures.

Section 3.3.2 Grazing-Incidence Small-Angle X-Ray Scattering

Grazing-incidence X-ray scattering has been demonstrated to be a powerful technique for studying polymer thin films.[3,18,46,52-54] In GISAXS, the scattering is acquired in the reflection geometry with incident angles near the critical angle of the film to minimize the contribution of the substrate to the scattering intensities.[51,52] With this technique, a quantitative measure of the mesostructure in organic semiconductor mixtures can be obtained. In this work, we focus on the in-plane data at the specular reflection and assume the Born Approximation is valid. Detector dark counts and empty-cell scattering are subtracted and data is normalized by the incident scattering intensity and the intensity of the scattered beam. Since our samples are composed of PBTTT:$PC_{71}BM$ films on top of PEDOT:PSS we model our films as being composed of two distinct layers. Scattering contributions of the PEDOT:PSS are subtracted using the procedure

outlined in the supplementary information, where the critical angle of 1:4 PBTTT/$PC_{71}BM$ thin films was found to be 0.141.

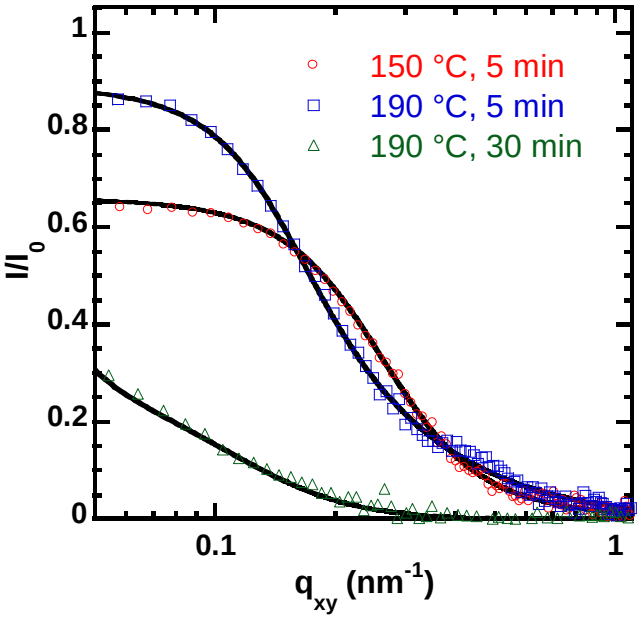

Figure 3 – 4: GISAXS intensity vs. scattering vector, *q*, for 1:4 PBTTT:$PC_{71}BM$ mixtures at various annealing conditions. The solid lines are Teubner-Strey fits to the data.

Figure 3 – 4 shows the GISAXS intensity as a function of the in-plane scattering vector, q_{xy}, for 1:4 PBTTT/$PC_{71}BM$ films at various annealing conditions. The intensity of the scattering curves that are annealed for 5 minutes have a drop in intensity at higher q values compared to the scattering curve of the film annealed for 30 min, indicating that domain spacing is increasing with annealing time. Describing this structural data quantitatively requires fitting to a model. The morphologies visible in Figure 3 – 2 are poorly ordered yet possess a characteristic length scale corresponding to PBTTT domains; visually, they resemble polymer microemulsions.[55] As shown by the solid curves in Figure 3 – 4, the use of the Teubner-Strey scattering function, originally developed for oil/water/microemulsions[56] and later extended to polymer blends,[57,58] describes the GISAXS data well over a wide *q*-range for samples annealed

at elevated temperatures. Thus, Teubner-Strey is an appropriate model for describing scattering from 1:4 PBTTT/$PC_{71}BM$ films.

In order to quantify the structure in polythiophene/fullerene mixtures, we fit the Teubner-Strey (T-S) scattering function to the GISAXS data. T-S was originally developed for bicontinuous microemulsions and is given by:[56]

$$I(q) = \frac{1}{a_2 + c_1 q^2 + c_2 q^4} + I_{bgd}(q) \tag{14}$$

where a_2, c_1, and c_2 are fitting parameters, q is the scattering vector, and $I_{bgd}(q)$ is a background function employed in polymeric systems. $I_{bgd}(q)$ is speculated to account for the connectivity of polymer chains and is assumed to be of the form $I_{bgd}(q) = (eq^2+f)^{-1}$, where e and f are fitting constants. [57,58] Fitting the GISAXS data to T-S yields the domain periodicity, d, correlation length, ξ_{TS}, and the amphiphilicity factor, f, through:

$$d = 2\pi\left[\frac{1}{2}\left(\frac{a_2}{c_2}\right)^{1/2} - \frac{1}{4}\frac{c_1}{c_2}\right]^{-1/2} \tag{15}$$

$$\xi_{TS} = \left[\frac{1}{2}\left(\frac{a_2}{c_2}\right)^{1/2} + \frac{1}{4}\frac{c_1}{c_2}\right]^{-1/2} \tag{16}$$

$$f = \frac{c_1}{\sqrt{4a_2c_2}} \tag{17}$$

since T-S is consistent with a real-space pair-correlation function, *g(r)*, given by:

$$g(r) = \frac{d}{2\pi r}\exp\left[-r/\xi_{TS}\right]\sin\left(\frac{2\pi r}{d}\right) \tag{18}$$

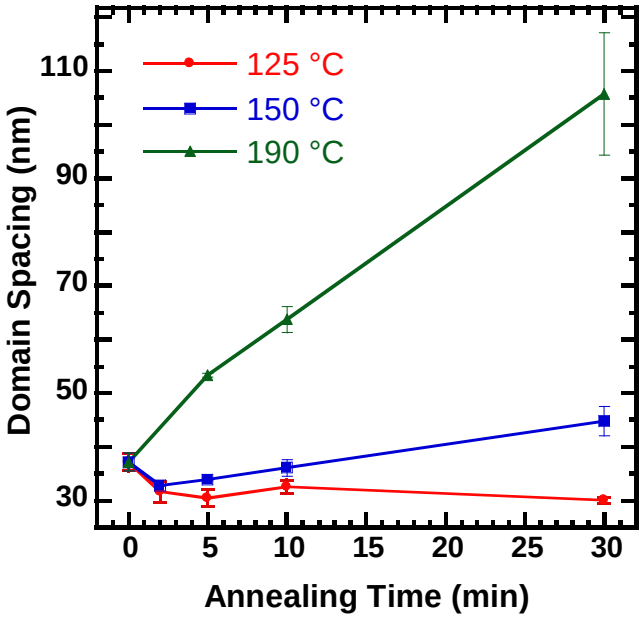

Figure 3 – 5: Domain spacings from GISAXS data of 1:4 PBTTT:$PC_{71}BM$ mixtures at various annealing conditions according to the Teubner-Strey model. Note that the domain spacing of films annealed at 150 °C and 190 °C increases with annealing time, whereas films annealed at 125 °C do not appear to demonstrate this behavior. Lines are guides to the eye. Error bars denote the standard deviation of multiple measurements.

Using Teubner-Strey as a model for the scattering data, the morphology in terms of the domain spacing, *d*, can be quantified. The melting point of the PBTTT, $PC_{71}BM$, and the bimolecular crystal has been reported as 232, 319, and 250 °C respectively.[70] We examined films annealed at 125, 150, and 190 °C for 2, 5, 10, and 30 min, as shown in Figure 3 – 5. Annealing at 125 °C appears to give a domain spacing of approximately 30 nm and has little change with annealing time over the range presented. However, annealing at 150 and 190 °C gives domain spacings that increase over time and range from approximately 30 to 100 nm.

These dramatic morphological changes make PBTTT/$PC_{71}BM$ mixtures an ideal candidate for correlating structure in terms of domain spacing to the efficiency of solar cell devices.

Section 3.4: The Structure-Function Relationship of 1:4 PBTTT/$PC_{71}BM$ Solar Cells

Section 3.4.1: A Simple Model to Predict the Effect of Domain Spacing On Performance

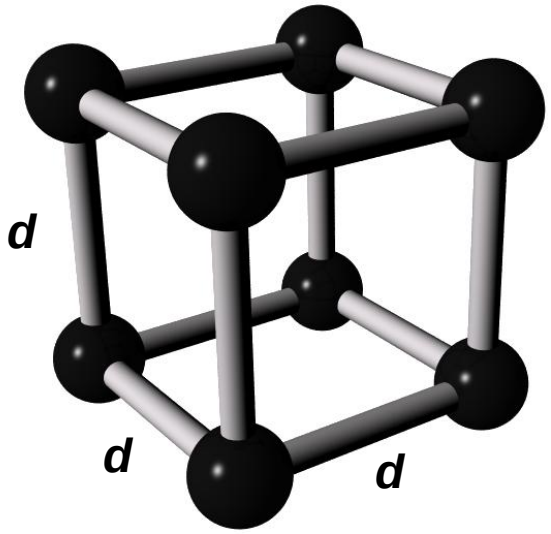

Figure 3 – 6: The polymer/fullerene mixture is modeled as spheres in a cubic lattice, where spheres represent polymer domains and the remaining area represents the amorphous fullerene concentrated domain. The domain spacing is taken to be the distance between spheres and the domain size is taken to be the diameter of a sphere.

A hypothesis for structure-function relationships in polythiophene/fullerene solar cells is formulated based on a simple model. Figure 3 – 6 models polymer/fullerene mixtures as spheres in a cubic lattice. Spheres represent polymer domains, where the remaining area is amorphous and concentrated with fullerene molecules. The domain spacing, *d*, is the distance between spheres and the radius of a sphere, *r*, is taken to be half the domain size. If we assume that the volume fraction of polymer domain remains constant with morphology changes, we can develop

a relationship between domain spacing and domain size. The volume fraction of the polymer domain is represented by,

$$\phi = \frac{\frac{4}{3}\pi r^3}{d^3} r \tag{19}$$

where ϕ is the volume fraction of polymer domain. Rearranging this equation gives,

$$d = \sqrt[3]{\frac{4\pi}{3\phi}} r \tag{20}$$

The volume fraction of polymer domain is taken to be 0.25 for 1:4 PBTTT/$PC_{71}BM$ mixtures. The conversion between the polymer domain size and domain spacing is useful because domain spacing is a direct result of the Teubner-Strey analysis, but the polymer domain size is hypothesized to correlate with device performance.

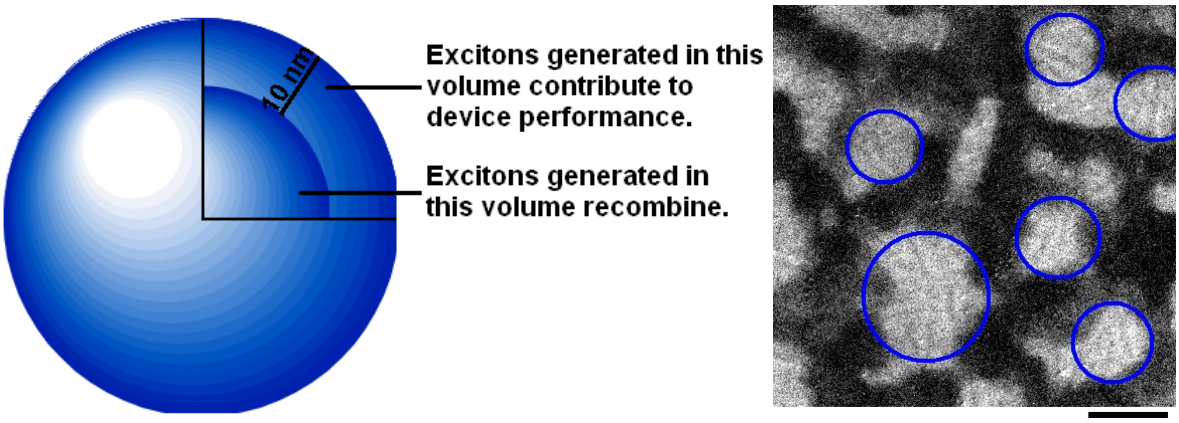

Figure 3 – 7: A simple model of polymer domains in the photoactive layer to aid in understanding the volume percentage of polymer that contributes to device performance. The sulfur map image identifies the areas of interest. Scale bar: 100 nm.

The domain spacing can be related to domain size via Equation 14. Figure 3 – 7 is used to develop a relationship between the domain size and the short circuit current of solar cell devices. Theoretically, the volume fraction of excitons that are harvested is directly proportional to the short circuit current of solar cell devices.[10,11] The polymer domain can be modeled as two concentric spheres, where the volume of the inner sphere generates excitons that recombine and the remaining volume generates excitons that dissociate at a polymer/fullerene interface, contributing to device performance. In reality, there is no clear cutoff between the volume that contributes to device performance and the volume that allows excitons to recombine, but it is clear that exciton diffusion is on the order of 10 nm.[22-25] Therefore, the outer sphere is taken to be 10 nm larger than the inner sphere as an approximation. This model also assumes that exciton diffusion is in the direction of high exciton concentration to low exciton concentration. According to this model, more than 50 % of polymer volume will contribute to device performance for domains that are smaller than 49 nm. We will show that the experimental data follows the trend predicted by this model when short circuit current is related to domain spacing.

Section 3.4.2: Solar Cell Device Data for 1:4 PBTTT/$PC_{71}BM$ Solar Cells

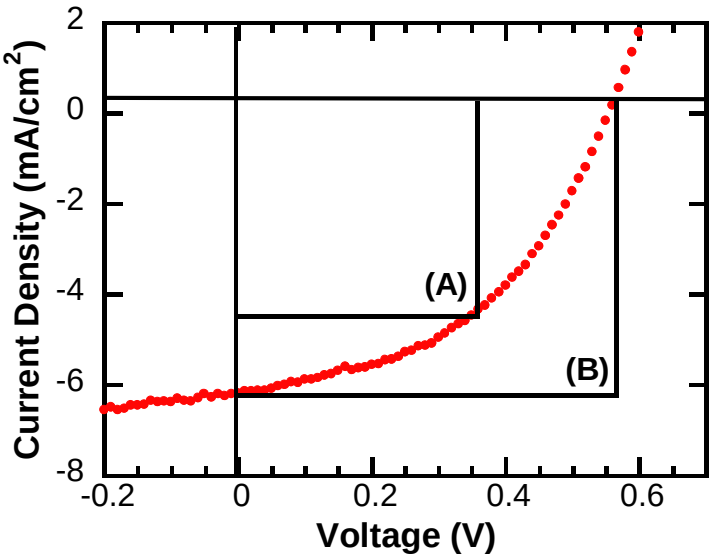

Figure 3 – 8: An example of a *J-V* curve. The solar cell active layer is 1:4 PBTTT/$PC_{71}BM$ annealed at 150 °C for 2 min. η = 1.58%.V_{OC} = 0.55 V. JSC = 6.19 mA/cm^2. FF = 0.46

Organic solar cells are typically characterized by a current, *J*, vs. voltage, *V*, curve that is taken during exposure to solar simulated light. Figure 3 – 8 shows a *J-V* curve for a 1:4 PBTTT/$PC_{71}BM$ bulk-heterojunction solar cell. Power is calculated by,

$$P = JV \tag{21}$$

and is represented by the area of the inner box in Figure 3 – 8. Power conversion efficiency is calculated by,

$$\eta = \frac{P_{max}}{P_I} \tag{22}$$

where P_{max} is the maximum power calculated from the data points on the J-V curve and P_I is the incident power of the solar simulator. The short circuit current, J_{SC}, is the current at which the voltage is 0. The open circuit voltage, V_{oc}, is the voltage at which the current is 0. The fill factor is a measure of how ideal the solar cell functions and is represented by ratio of the area of the small box (A) to the area of the large box (B) in Figure 3 – 8.[10,11]

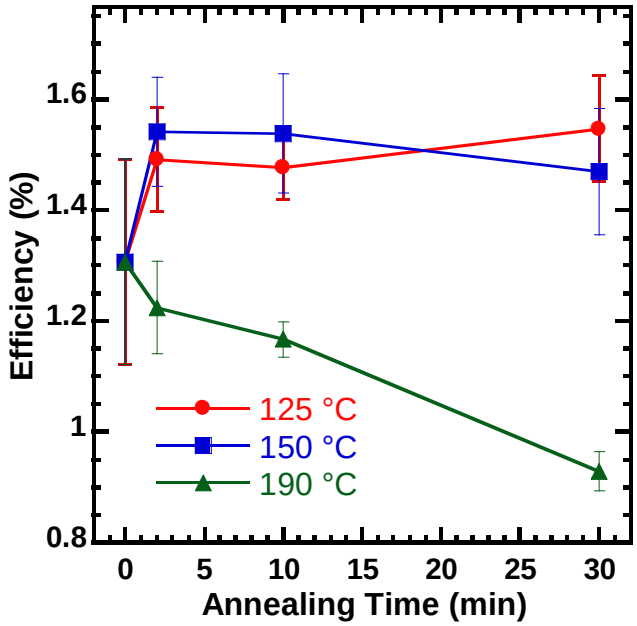

Figure 3 – 9: Efficiency vs. time for 1:4 PBTTT/PC_{71}BM solar cells at various annealing conditions.

Solar cell performance results in terms of device efficiency are summarized in Figure 3 – 9. Annealing conditions have a significant affect on device performance and it is apparent that higher annealing temperatures such as 190 °C lead to poor performance. Figures 3 – 2 and 3 – 5 show that dramatic changes in the morphology occur at higher temperatures, which has a clear and direct connection to the device performance: larger domains are the cause of poor performance in 1:4 PBTTT/PC_{71}BM solar cell devices. The structure can also be quantitatively related to device performance in terms of efficiency based on the domain spacing calculated by the Teubner-Strey model.

Section 3.4.3: Comparison of the Simple Model with Experimental Data

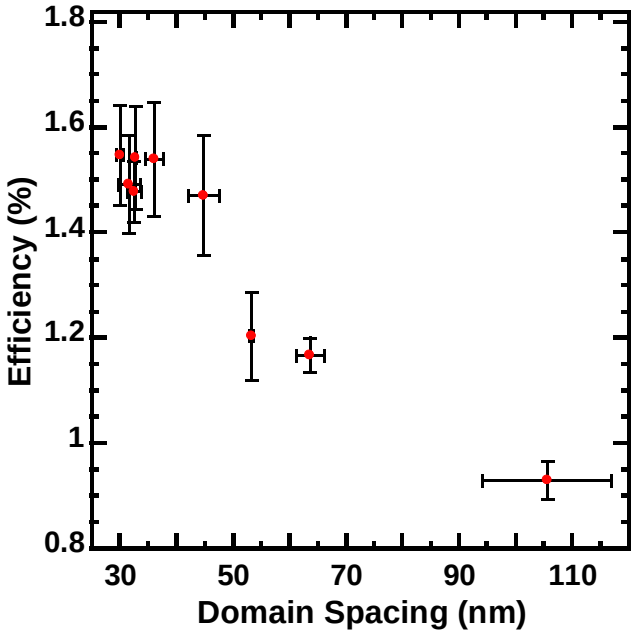

Figure 3 – 10: Efficiency vs. Domain Spacing for 1:4 PBTTT/$PC_{71}BM$ Solar Cells. Domain spacing is a direct result of the Teubner-Strey analysis.

One of the important guiding principals for studying organic solar cells is the idea that exciton recombination can limit the performance of a device. It has been reported that exciton diffusion is efficient for approximately 10 nm.[22-25] Thus, the hypothesis that many researchers formulate is that smaller polymer domains will give better device efficiencies.[10,11,16,17,23-25,31] However, this phenomenon has never been proven quantitatively until now. The 1:4 PBTTT/$PC_{71}BM$ mixture is an ideal candidate for developing a structure-function relationships because of its large range of domain spacings. Figure 3 – 10 demonstrates the inverse relationship between the domain spacing of 1:4 PBTTT/$PC_{71}BM$ thin films and the solar cell device efficiency at similar annealing conditions.

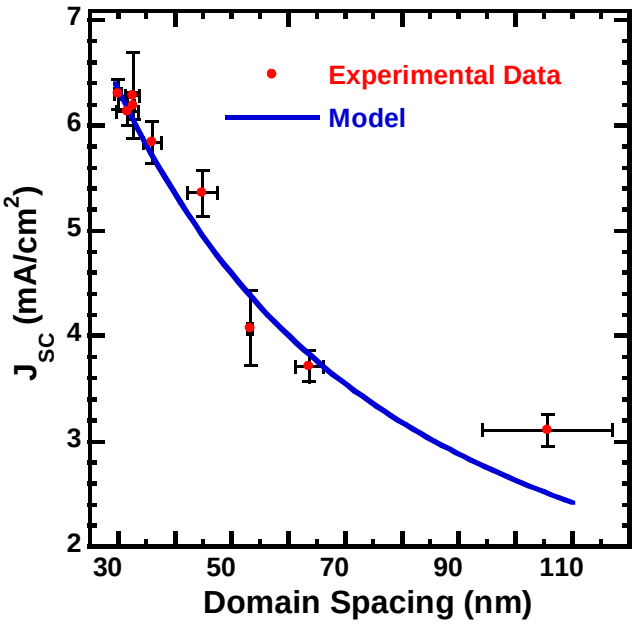

Figure 3 – 11: Short Circuit Current vs. Domain Spacing for 1:4 PBTTT/$PC_{71}BM$ Solar Cells. Domain spacing is a direct result of the Teubner-Strey analysis.

Figure 3 – 11 shows the short circuit current versus domain spacing for 1:4 PBTTT/$PC_{71}BM$ solar cells. In an organic solar cell, the short circuit current is proportional to the rate of exciton harvesting.[10,11] The experimental data matches well with the theoretical model, suggesting that the proposed mechanism for exciton harvesting is true. The trend is similar to the one seen in Figure 3 – 10, revealing that the varying efficiency of 1:4 PBTTT/$PC_{71}BM$ solar cells is controlled by changes in the short circuit current.

The PBTTT/$PC_{71}BM$ mixture is unique in that it has a very large range of domain spacings compared to other polythiophene/fullerene mixtures. If these results are universal for all polythiophene/fullerene solar cells, the trend in Figure 3 – 11 has large implications for 1:1 P3HT/PCBM systems. Figure 2 – 5 shows that 1:1 P3HT/PCBM mixtures have domain spacings in the range of 26 – 34 nm for films annealed at 100, 140, 165, 190 °C for 5, 10, 30, and 60 min. Based on these results, it appears that domain spacing does not have a dominating effect

on device performance in 1:1 P3HT/PCBM mixtures. According to Figure 3 – 11, an increase in domain spacing from 26 nm to 34 nm corresponds to a 12% decrease in short circuit current. A 12% decrease in efficiency is minimal compared to the fluctuations in device performance that are typically seen in organic solar cells.[10,11,17]

Section 3.5: Summary and Conclusions

EFTEM and GISAXS have been used to show that 1:4 PBTTT:$PC_{71}BM$ mixtures have a complex morphology with up to 4 levels of structure: micron-sized fullerene clusters, a mesostructure of PBTTT and $PC_{71}BM$ domains, a structure on the order of 10-20 nm within PBTTT domains, and a molecular structure due to intercalation. The mesoscale structure was characterized quantitatively in terms of the domain spacing based on the Teubner-Strey model. It was hypothesized that the domain spacing would be related to the short circuit current of solar cell devices based on a simple geometric model. This hypothesis was confirmed to be true, where increases in the domain spacing lead to decreases in the short circuit current. In previous works, it has been speculated that polymer domains must be on the order of 20 nm for efficient exciton harvesting.[10,17,31] Our results suggest that the in-plane morphology does not have a dominant effect on device performance for polymer/fullerene systems that have domain spacing ranges less than 10 nm, such as the P3HT/PCBM system. Therefore, future experiments involving P3HT/PCBM mixtures should focus on other properties of the photoactive layer that have been hypothesized to affect device performance, such as vertical phase separation, polymer light absorption, and mobility characteristics in each phase.[10,11] Also, the design of PBTTT/$PC_{71}BM$ solar cells should be approached with caution because the wide range of domain spacings allows for a wide range of device performance.

Chapter 4: Future Work

Chapter 4.1: Structure-Function Relationships in P3HT/PCBM Bulk-Heterojunction Solar Cells

Section 4.1.1: Introduction and Theory

One of the important guiding principals in the field of polymer/fullerene solar cells is the understanding of exciton diffusion length in conductive polymers. Previous work has estimated the exciton diffusion length in conductive polymers to be on the order of 10 nm.[22-25] This leads to the hypothesis that larger domains promote exciton recombination in the polymer and do not use the material to its full capability in generating an electric current. This can be shown qualitatively when bilayer solar cells are compared to bulk-heterojunction solar cells. Although there are many factors that contribute to device performance, the bulk-heterojunction architecture is thought to give better performance because it allows for smaller domains which prevent exciton recombination and make more efficient use of material.[9,11] For a more complete understanding of polymer/fullerene solar cells, it would be advantageous to quantitatively describe this phenomenon. The theory behind the conversion mechanism of organic solar cells suggests that a characteristic length scale, such as domain size or domain spacing, should correlate to a device performance parameter, such as short circuit current or efficiency. Our hypothesis is that the domain spacing is inversely correlated to device efficiency.

Section 4.1.2: Experimental Methods

Solutions of regioregular P3HT (96% H-T regioregular, M_n = 28 kg/mol, polydispersity = 1.9, Merck) and PCBM (>99.5%, Nano-C) were made with anhydrous chlorobenzene (Sigma-Aldrich) in a N_2 glovebox. Solutions were stirred for a minimum of 1 hr and heated to 100 °C for 10 seconds prior to use to ensure dissolution.

Solar cells were fabricated on Indium Tin Oxide (ITO) coated glass substrates (Kintec). The substrates were cleaned with Aquet detergent solution and water, followed by 10 min of sonication in acetone and isopropanol and 10 min of UV-ozone treatment. PEDOT:PSS was spun cast in a laminar flow hood at 4000 rpm for 2 min and subsequently dried at 165 °C for 10 min. The active layer was spun cast in a N_2 glovebox at 1000 rpm for 1 min. A 75 nm layer of aluminum was applied via thermal deposition.

Solar cell performance was tested by generating a current vs. voltage curve when exposed to 1.5 AM (0.1 W/cm^2) light from a solar simulator (Newport Model SP92250A-1000). Voltage is applied and current is measured by the Keithley 2636A Sourcemeter.

Section 4.1.3: Analysis and Results

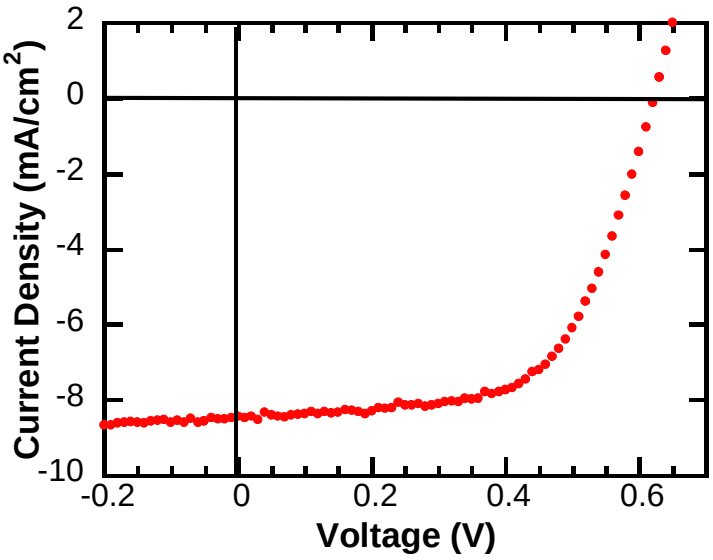

Figure 4 – 1: An example of a *J-V* curve. The solar cell active layer is 1:1 P3HT/PCBM annealed at 165 °C for 10 min. η = 3.3%.V_{OC} = 0.62 V. JSC = 8.48 mA/cm^2. FF = 0.6202

Organic solar cells are typically characterized by a current, *J*, vs. voltage, *V*, curve that is taken during exposure to solar simulated light. Figure 4 – 1 shows a *J-V* curve for a 1:1 P3HT/PCBM bulk-heterojunction solar cell. Power is calculated by,

$$P = JV \tag{23}$$

and power conversion efficiency is calculated by,

$$\eta = \frac{P_{max}}{P_I} \tag{24}$$

where P_{max} is the maximum power calculated from the data points on the J-V curve and P_I is the incident power of the solar simulator.

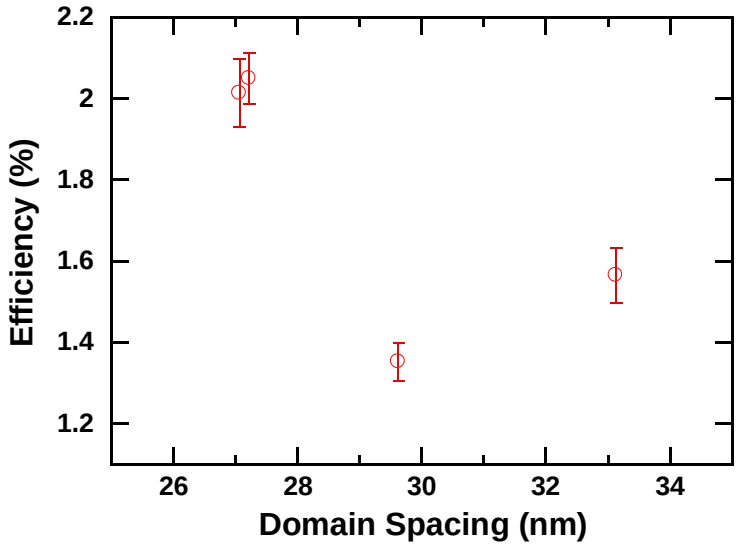

Figure 4 – 2: Efficiency vs. Domain Spacing for 10 min anneal times. No correlation is apparent.

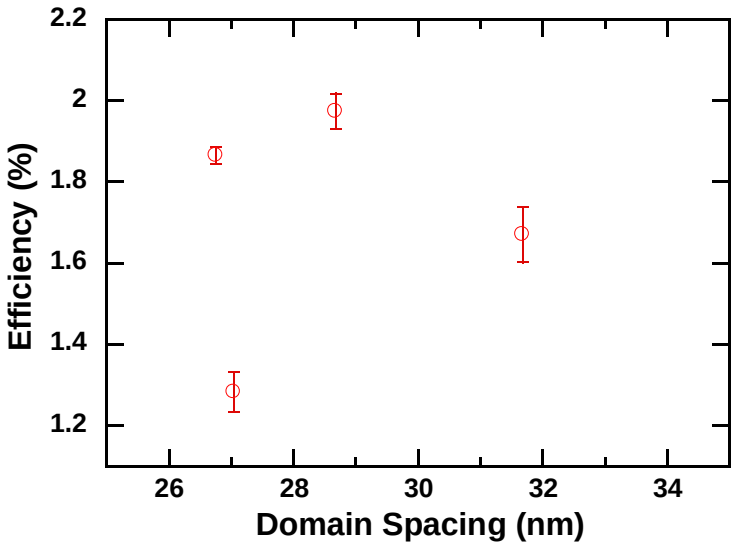

Figure 4 - 3: Efficiency vs. Domain Spacing for 30 min anneal times. No correlation is apparent.

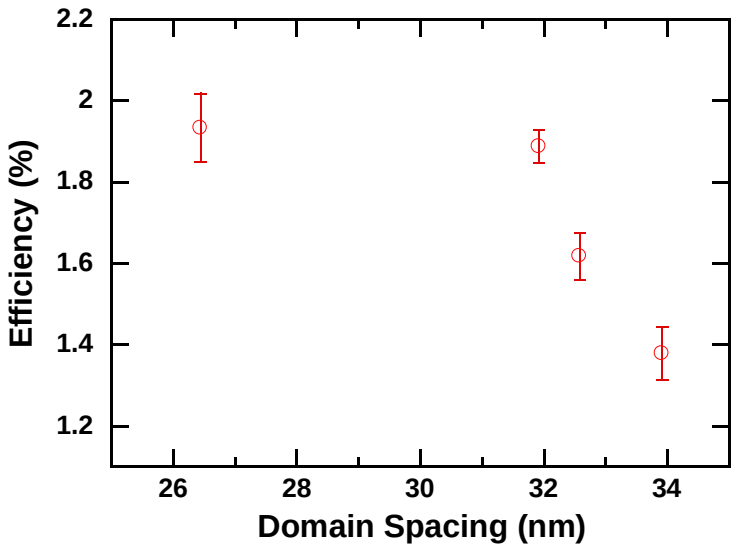

Figure 4 – 4: Efficiency vs. Domain Spacing for 60 min anneal times. The efficiency appears to be inversely correlated to the domain spacing after 30 nm.

Device performance was characterized using the same processing conditions as seen in the domain spacing results in Figure 2 – 5. The device performance was then plotted against domain spacing for three annealing times: 10 min, 30 min, and 60 min. When an annealing time of 10 min or 30 min is used, there is no correlation between efficiency and domain spacing. However, the three data points beyond 30 nm in Figure 4 – 4 appear to give an inverse relationship between efficiency and domain spacing. Although these data points appear to be correlated, the slope is much sharper than is expected (see Section 3.4). Thus, the results are inconclusive due to the small range of domain spacings over the annealing conditions studied (~26 – 34 nm). Future experiments should be designed so that higher domain spacings are achieved. This will require annealing for longer times at lower temperatures, such as 100 °C and 140 °C, which give higher domain spacings in Figure 2 – 5. Lowering the concentration of P3HT may also lead to higher domain spacing.

Section 4.2: The Shadow FIB characterization method for use in bulk-heterojunction polymer/fullerene solar cells

Section 4.2.1: Introduction and Background

TEM sample preparation is very important when studying P3HT/PCBM mixtures.[2,17,19,31] The goal of our TEM sample preparation is to emulate the conditions seen in the active layer organic solar cells. Currently, the most successful sample preparation method has been floating films of P3HT/PCBM in distilled water as noted in Chapter 2. This method ultimately falls short of obtaining an accurate measurement of the active layer in organic solar cells for a simple reason; the interfacial effects between the active layer and its bordering layers are neglected. Also, this type of sample preparation is only useful for studying the in-plane morphology, and cannot describe vertical phase separation. Ideally, we would like to mill an actual solar cell to electron transparency and use EFTEM techniques to generate images with high contrast. Typically, this type of milling is done in a Focused Ion Beam (FIB).[31,71,72] However, it has been shown that traditional FIB techniques, such as the lift-out method, will damage polymer films.[6,73] Therefore, we propose the use of the shadow FIB technique, where the ion beam never contacts the active layer and cuts the glass first in an effort to prevent damage and heating to the polymer mixture.[6,74] For organic solar cells, it is imperative that this is done with great caution because local heating effects can also change the morphology of the active layer.

Direct imaging of solar cells has many advantages over studying films floated in distilled water. Solar cell performance data is readily available for that specific cell, so correlating device performance to morphology becomes much more direct. It is also a very useful technique for failure analysis. Solar cells sometimes function poorly because of vertical phase separation,

which is typically seen as a pure layer of P3HT or PCBM resting upon the interface of PEDOT:PSS or the aluminum electrode.

The change in temperature for areas exposed to the ion beam, *T*, can be estimated using,

$$T = \frac{P}{\pi a k} \tag{25}$$

where *P* is the power of the ion beam, *a* is the radius of the circular ion beam profile, and *k* is the thermal conductivity of the material. It has been shown that local heating effects in polymers are a thousand times higher than that of metals.[6]

Section 4.2.2: Experimental Methods

Solar cells were prepared according to the procedure in Section 4.1.2. Each solar cell device was separated from the substrate using a scribe. After choosing a device of interest, small scratches were made on the bottom of the glass substrate and the device was smashed with a hammer. Shards that contain all of the layers in the solar cell can be identified by the presence of aluminum, which will reflect light. A shard of interest was attached to a VECO handle specimen grid using a strong adhesive in such a way that the cross section can be readily viewed with little titling in a TEM. The glass portion of the shard was covered in carbon paint to eliminate charging.

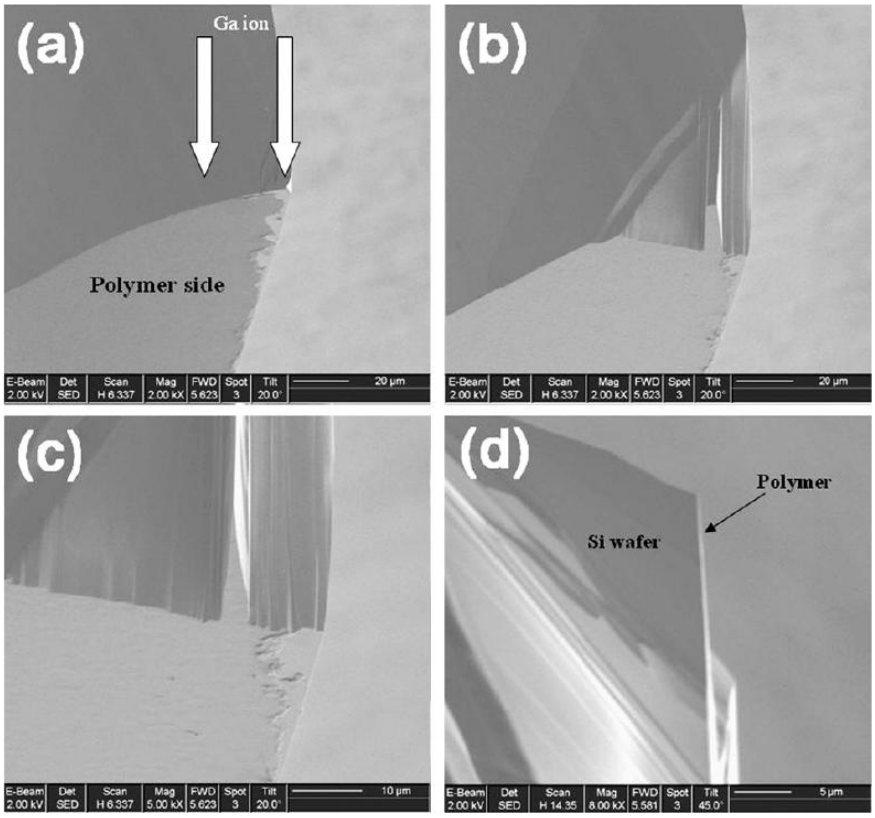

Figure 4 – 5: The Shadow-FIB method from "Minimization of focused ion beam damage in nanostructured polymer thin films" by Kim et al. SEM images a – c show the progression of the Shadow-FIB technique throughout the milling process. SEM image d shows the cross-section view after milling was completed.[6]

The Shadow FIB technique was used to mill the solar cell to electron transparency. Shadow-FIB minimizes beam damage by cutting the glass first and never exposes the polymer film to a direct ion beam. The sample should be oriented so the gallium gun can make a 30 - 45° cut as shown in Figure 4 – 5. SEM imaging is avoided whenever possible and the gallium gun is limited to low currents (approximately 100 pA) when viewing. Voltage is generally kept constant at 30 kV. Larger cuts may require higher currents, but it is imperative to limit the current as much as possible. Within a micron of the area of interest, the current should be below 100 pA. Thus, it is advantageous for a shadow FIB sample to come to a point at an acute angle, as seen in Figure 4 – 5. This minimizes the amount of milling needed to create an electron transparent sample. Final cuts were made using 10 pA or less.

Section 4.2.3: Results and Discussion

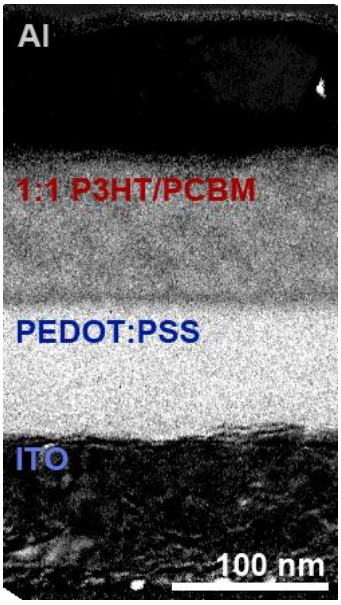

Figure 4 – 6: Sulfur map of a 1:1 P3HT/PCBM solar cell cross section prepared by the Shadow-FIB method. Mesostructure is not clearly visible. However, an interfacial layer of PCBM is observed between the PEDOT:PSS and the active layer.

Figure 4 – 6 shows sulfur map of a 1:1 P3HT/PCBM solar cell cross section annealed at 165 °C for 10 min prepared by the Shadow FIB method. The structure within the active layer appears to be much more diffuse compared to the images in Figure 2 – 1. It is unclear whether this happens because of beam damage or if this is the true morphology of the active layer when aluminum and PEDOT:PSS are present. Future experiments should test highly ordered systems, such as those annealed at 190 °C, for similarities and differences between the films in Figure 2 – 1 and the morphology that is apparent after milling via the shadow FIB method. If this structure does not become apparent, it is likely that local heating is destroying the morphology and cryo-FIB may be necessary.

Although it is unclear whether the structure of the active layer is preserved by using the shadow-FIB technique for organic solar cells, it is clear that vertical phase separation is. A dark layer between the active layer and PEDOT:PSS is visible in Figure 4 – 6, indicating a deficiency

of sulfur. This layer is presumably PCBM. PCBM is an electron transporting material and this is a very important interface for hole transport. The presence of a PCBM layer at this junction can greatly slow the transport of holes and thus limit the efficiency of the device. This device had a low efficiency (< 0.1 %) and this is likely one of the major reasons. Therefore, studying vertical phase separation via the Shadow-FIB technique can be very good for failure analysis, but it is unclear whether or not this technique may be used for robust morphological characterization.

Section 4.3: Electric field alignment of P3HT fibers in an amorphous P3HT/PCBM matrix

Section 4.3.1: Introduction and Background

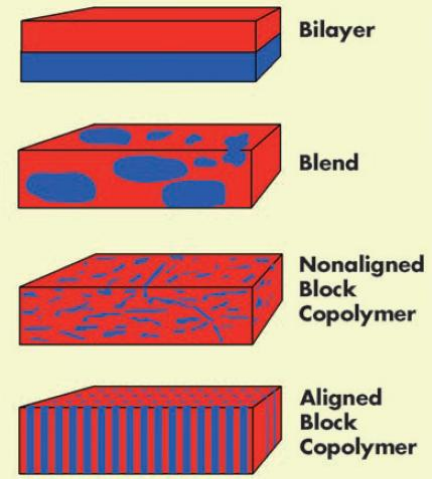

Figure 4 -7: Various morphologies for Donor:Acceptor organic solar cells from "Charge separation at self-assembled nanostructured bulk interface in block copolymers" by Linder et al.[7]

Understanding the morphology of 1:1 P3HT:PCBM mixtures creates many opportunities for perturbing the structure. The bulk-heterojunction architecture inherently creates a tortuous transport path for electrons and holes. Theoretically, this increases the probability for electron-hole recombination and thus lowers the efficiency of organic solar cells. It has been speculated

that the ideal morphology for polymer/fullerene solar cells is a lamellar or cylindrical structure with domains on the order of 10 nm that starts at one charge collection interface and ends at another as seen in Figure 4 - 7.[7,75-77] Many groups attempt to achieve this architecture by using block copolymers, which give much lower efficiencies than the well-studied P3HT:PCBM system.[7,75-78]

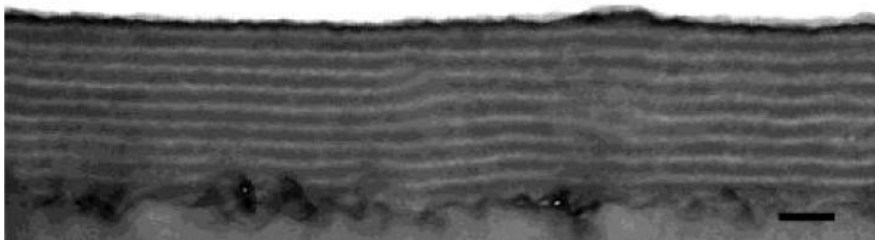

Figure 4 – 8: Cross sectional TEM image of polystyrene-*b*-poly(methyl methacrylate) annealed under a 40 V/μm electric field for 6 hours. The electric field vector is parallel to the lamellae structures from "Electric field alignment of asymmetric diblock copolymer thin films" by Xu et al. Scale bar: 100 nm[8]

Alignment of block copolymers has been achieved by the use of external fields.[8,79-86] In particular, electric fields have proven to be useful in aligning lamellar or cylindrical structures that form in polymer films.[8,79-82] Alignment occurs because of an anisotropic contribution to the free energy of a dielectric material in an electric field, in which the minimum free energy state is the configuration where lamellae or cylindrical structures align parallel to the electric field vector.[79,80,87] The driving force behind this process is the difference in permittivity for the two materials in the system.[79,80] In 1:1 P3HT:PCBM films annealed at 190 °C, cylindrical crystalline structures of pure P3HT are embedded in a matrix of an amorphous P3HT:PCBM mixture, as seen in Figure 2 – 1. The permittivity constants for P3HT and PCBM are approximated to be, 3.0[88,89] and 3.9[89,90] respectively. This system presents a promising initial architecture to achieve the morphology that is seen in aligned block copolymers, but has the advantage of using a mixture that has been proven to work well in organic solar cell devices.

Section 4.3.2: Experimental Methods

1:1 P3HT/PCBM solar cells were fabricated according to the procedure in section 4.1.2. Out of the six devices present on a substrate, only one was exposed to an electric field and all others served as a control. A heating stage on a probe station was heated to 190 °C. The solar cell was placed on the hot plate and the probes were connected to the ITO and to the aluminum within 30 seconds. Immediately, a DC voltage of 5 V, 10 V, or 50 V then applied for 10 min. The current was measured as a function of time during the annealing process. Solar cells were tested and characterized according to the procedure in Section 4.1. The active layer solution was prepared as a 1:1 P3HT/PCBM mixture at 35 mg/mL in chlorobenzene. Spin coating of the active layer was done at 800 rpm.

Section 4.3.3: Results and Discussion

Bias	Efficiency With Electric Field	Efficiency Without Electric Field
5 V	2.51	2.5 ± 0.10
10 V	2.45	2.34 ± 0.13
50 V	0.71	2.38 ± 0.20

Table 4 -1: Performance of 1:1 P3HT PCBM solar cells after annealing at 190 °C for 10 min under an electric field.

Theoretically, an electric field bias will align the cylindrical crystal structures that form at 190 °C. This allows for a less tortuous pathway for electron and hole transport within the active layer of organic solar cells, thus enhancing performance. Annealing for 10 min while exposed to a voltage bias does not give significant improvement in the performance of organic solar cells. As shown in Table 4 – 1, annealing while exposed to 5 V and 10 V biases gives power conversion efficiencies that are within the error when the solar cell is not exposed to an electric field. Annealing while exposed to a 50 V bias significantly lowers the power conversion efficiency of the cell, which suggests that degradation of the polymer has occurred. For future experiments, longer annealing times should be used at lower voltages (5 – 10 V).

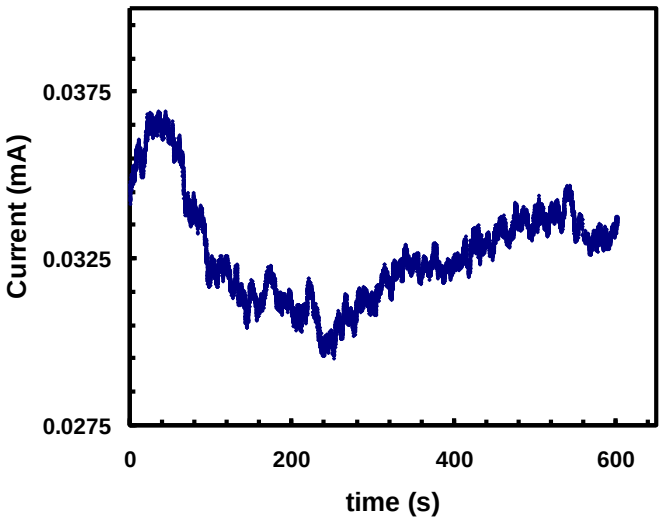

Figure 4 – 9: Current vs. time during 10 min of annealing at 190 °C under 5 V bias.

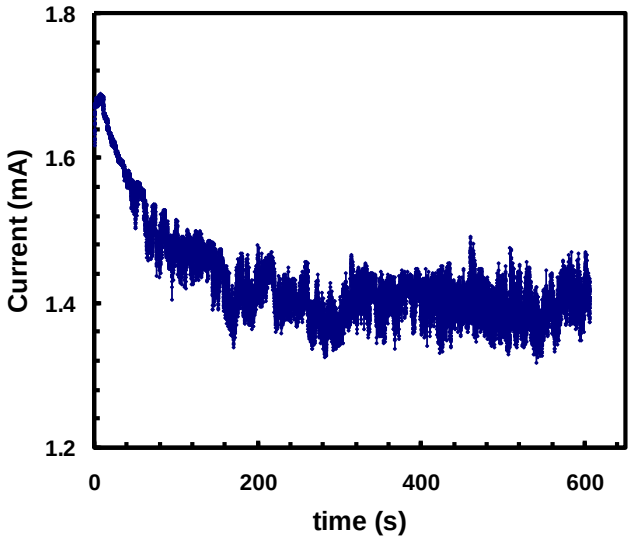

Figure 4 – 10: Current vs. time during 10 min of annealing at 190 °C under a 10 V bias.

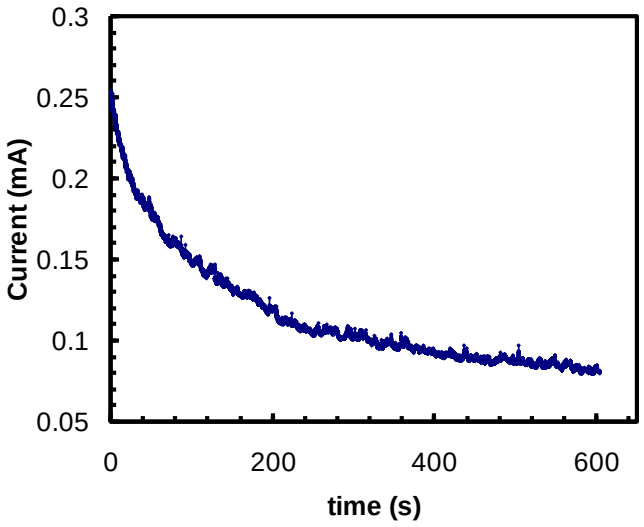

Figure 4 – 11: Current vs. time during 10 min of annealing at 190 °C under a 50 V bias.

Previous works have presented the successful alignment of block copolymers using a 10 - 40 V/μm bias during thermal annealing.[8,81,82] The films used in this experiment are approximately 280 nm thick, including PEDOT:PSS. Thus, a 5 – 10 V bias is within the proper range for alignment without damaging the polymer, which is supported by the current vs. time curves in Figures 4 – 9, 4 – 10, and 4 – 11. Measuring the current during thermal annealing when the voltage bias is applied can help characterize the effect of the electric field within the active layer. Applying a 5 or 10 V bias gives a peak in the current at short annealing times. All voltage biases exhibit decay in the current from 1 to 5 min. This decay continues when 10 V and 50 V are applied, but the current rises from 5 to 10 min when 5 V are applied. Thus, applying a 5 V bias during thermal annealing appears to have an effect on the electrical properties of the active layer, which suggests that a morphology change may be occurring. To further study the effects of a 5 V bias, longer annealing times should be used in an effort to increase the current as much as possible. It may also be advantageous to remove the voltage bias at one of the peaks in current seen at shorter annealing times. The Focused Ion Beam characterization method in

Section 4.2 may be used to confirm the alignment of P3HT fibers within the active layer of these devices.

Chapter 5: Summary and Outlook

We have used novel characterization methods to examine the structure of the active layer in organic solar cells. Energy Filtered Transmission Electron Microscopy (EFTEM) was used to capture images of polythiophene/fullerene mixtures with high contrast between domains. EFTEM was also useful in determining domain compositions. Grazing-Incidence Small-Angle X-Ray Scattering was also used in conjunction with the Teubner-Strey scattering model to determine the domain spacing of the active layer at various processing conditions.

DSC experiments were also used to determine the extent of miscibility of P3HT/PCBM films, which aided in determining the mechanism of structure formation in these mixtures upon thermal annealing. P3HT controls structure formation in the sense that pure domains form upon crystallization. The amorphous mixed domain is then depleted of P3HT. If enough P3HT is taken out of the amorphous phase, the concentration of PCBM may reach its miscibility limit and precipitate out as a pure PCBM phase.

Structure-function relationships for polythiophene/fullerene solar cells were also explored. In 1:4 PBTTT/$PC_{71}BM$ mixtures, large scale phase separation lead to a decrease in solar cell performance. This was confirmed by a model where the outer 10 nm of a polymer domain was said to contribute to the device performance and the remaining volume generates excitons that recombine. The data suggests that the in-plane morphology is not a performance limiting characteristic for solar cells with small domain spacing ranges (~10 – 20 nm), such as the 1:1 P3HT/PCBM mixture. Structure-function relationships were also explored for P3HT/PCBM mixtures. However, the results were inconclusive due to the small domain spacing range in 1:1 P3HT/PCBM system. This data suggests that the in-plane morphology is not the dominating factor in determining device efficiency.

EFTEM and GISAXS are excellent methods for examining the structure of the active layer in organic solar cells, but they fall short of a complete characterization because they cannot examine vertical phase separation well. Ultimately, this research will have to focus on determining the vertical phase separation in polymer/fullerene mixtures and this can be achieved by making cross sections of a solar cell in a focused ion beam (FIB).

Finally, a large component of future research should focus on morphology control. There are many tools that can be used to manipulate the structure of the active layer to a configuration that optimizes charge transport. EFTEM images show that a large amount of morphology control can be achieved by changing simple experimental parameters such as the ratio of polymer to fullerene, annealing time, and annealing temperature. Also, since it has been shown that polymer crystallization is the main driving force behind structure formation, polymer properties such as molecular weight and regioregularity can play a very important role in morphology control. The extent to which the polymer crystallizes is critical in the structure formation process. Thus, controlling crystal nucleation is important, which may be achieved by adding a third component that aids in creating nucleation sites for crystallization. Furthermore, external fields, such as an electric field, may be used during the thermal annealing process to control the orientation of polymer crystals.

References

1 **Kazmerski, L. (National Renewable Energy Laboratory, 2010).**

2 **van Bavel, S. S., Sourty, E., de With, G. & Loos, J. Three-Dimensional Nanoscale Organization of Bulk Heterojunction Polymer Solar Cells. *Nano Lett.* 9, 507-513, doi:10.1021/nl8014022 (2009).**

3 **Gomez, E. D., Barteau, K. P., Wang, H., Toney, M. F. & Loo, Y.-L. Correlating the scattered intensities of P3HT and PCBM to the current densities of polymer solar cells. *Chemical Communications* 47, 436-438 (2011).**

4 **Chen, C. H. *et al.* Alternating and Diblock Donor-Acceptor Conjugated Polymers Based on Diindeno 1,2-b:2 ',1 '-d thiophene Structure: Synthesis, Characterization, and Photovoltaic Applications. *Chem.-Asian J.* 5, 2483-2492, doi:10.1002/asia.201000506 (2010).**

5 **Cates, N. C. *et al.* Tuning the Properties of Polymer Bulk Heterojunction Solar Cells by Adjusting Fullerene Size to Control Intercalation. *Nano Lett.* 9, 4153-4157, doi:10.1021/nl9023808 (2009).**

6 **Kim, S., Park, M. J., Balsara, N. P., Liu, G. & Minor, A. M. Minimization of focused ion beam damage in nanostructured polymer thin films. *Ultramicroscopy* 111, 191-199, doi:10.1016/j.ultramic.2010.11.027 (2011).**

7 **Lindner, S. M., Huttner, S., Chiche, A., Thelakkat, M. & Krausch, G. Charge separation at self-assembled nanostructured bulk interface in block copolymers. *Angew. Chem.-Int. Edit.* 45, 3364-3368, doi:10.1002/anie.200503958 (2006).**

8 **Xu, T. *et al.* Electric field alignment of asymmetric diblock copolymer thin films. *Macromolecules* 38, 10788-10798, doi:10.1021/ma050221c (2005).**

9 **Brabec, C. J. *et al.* Polymer-Fullerene Bulk-Heterojunction Solar Cells. *Advanced Materials* 22, 3839-3856, doi:10.1002/adma.200903697 (2010).**

10 **Li, G., Shrotriya, V., Yao, Y., Huang, J. & Yang, Y. Manipulating regioregular poly(3-hexylthiophene) : [6,6]-phenyl-C61-butyric acid methyl ester blends—route towards high efficiency polymer solar cells. *Journal of Materials Chemistry* 17, 3126, doi:10.1039/b703075b (2007).**

11 **Thompson, B. C. & Fréchet, J. M. J. Polymer–Fullerene Composite Solar Cells. *Angewandte Chemie International Edition* 47, 58-77, doi:10.1002/anie.200702506 (2008).**

12 ***UD-led team sets solar cell record, joins DuPont on $100 million project,* <http://www.udel.edu/PR/UDaily/2008/jul/solar072307.html> (2007).**

13 ***Understanding the Cost of Solar Energy*, <http://greenecon.net/understanding-the-cost-of-solar-energy/energy_economics.html> (2007).**

14 ***Konarka Powerplastic* <http://www.konarka.com/index.php/power-plastic/about-power-plastic/> (2010).**

15 **Dennler, G. in *American Physical Society March Meeting.* (Konarka).**

16 **Li, G. *et al.* High-efficiency solution processable polymer photovoltaic cells by self-organization of polymer blends. *Nature Materials* 4, 864-868, doi:10.1038/nmat1500 (2005).**

17 **Ma, W., Yang, C., Gong, X., Lee, K. & Heeger, A. J. Thermally Stable, Efficient Polymer Solar Cells with Nanoscale Control of the Interpenetrating Network**

Morphology. ***Advanced Functional Materials*** **15, 1617-1622, doi:10.1002/adfm.200500211 (2005).**

18 Woo, C. H., Thompson, B. C., Kim, B. J., Toney, M. F. & Frechet, J. M. J. The Influence of Poly(3-hexylthiophene) Regioregularity on Fullerene-Composite Solar Cell Performance. ***Journal of the American Chemical Society*** **130, 16324-16329, doi:10.1021/ja806493n (2008).**

19 Xin, H. ***et al.*** **Polymer Nanowire/Fullerene Bulk Heterojunction Solar Cells: How Nanostructure Determines Photovoltaic Properties.** ***ACS Nano*** **4, 1861-1872, doi:10.1021/nn9014906 (2010).**

20 Yang, F., Shtein, M. & Forrest, S. R. Controlled growth of a molecular bulk heterojunction photovoltaic cell. ***Nature Materials*** **4, 37-41, doi:10.1038/nmat1285 (2005).**

21 Forrest, S. R. The limits to organic photovoltaic cell efficiency. ***MRS Bull.*** **30, 28-32 (2005).**

22 Haugeneder, A. ***et al.*** **Exciton diffusion and dissociation in conjugated polymer fullerene blends and heterostructures.** ***Phys. Rev. B*** **59, 15346-15351 (1999).**

23 Huijser, A., Savenije, T. J., Shalav, A. & Siebbeles, L. D. A. An experimental study on the molecular organization and exciton diffusion in a bilayer of a porphyrin and poly(3-hexylthiophene). ***J. Appl. Phys.*** **104, doi:034505 10.1063/1.2958325 (2008).**

24 Shaw, P. E., Ruseckas, A. & Samuel, I. D. W. Exciton diffusion measurements in poly(3-hexylthiophene). ***Advanced Materials*** **20, 3516-+, doi:10.1002/adma.200800982 (2008).**

25 Wang, H. ***et al.*** **Exciton diffusion and charge transfer dynamics in nano phase-separated P3HT/PCBM blend films.** ***Nanoscale*** **3, 2280-2285, doi:10.1039/c0nr01002b (2011).**

26 Brinkmann, M. & Rannou, P. Effect of molecular weight on the structure and morphology of oriented thin films of regioregular poly(3-hexylthiophene) grown by directional epitaxial solidification. ***Advanced Functional Materials*** **17, 101-108, doi:10.1002/adfm.200600673 (2007).**

27 Campoy-Quiles, M. ***et al.*** **Morphology evolution via self-organization and lateral and vertical diffusion in polymer:fullerene solar cell blends.** ***Nature Materials*** **7, 158-164, doi:10.1038/nmat2102 (2008).**

28 Chiu, M. Y., Jeng, U. S., Su, C. H., Liang, K. S. & Wei, K. H. Simultaneous use of small- and wide-angle X-ray techniques to analyze nanometerscale phase separation in polymer heterojunction solar cells. ***Advanced Materials*** **20, 2573-+, doi:10.1002/adma.200703097 (2008).**

29 Kiel, J. W., Eberle, A. P. R. & Mackay, M. E. Nanoparticle Agglomeration in Polymer-Based Solar Cells. ***Phys. Rev. Lett.*** **105, doi:168701 10.1103/PhysRevLett.105.168701 (2010).**

30 Kim, J. Y. & Frisbie, D. Correlation of Phase Behavior and Charge Transport in Conjugated Polymer/Fullerene Blends. ***J. Phys. Chem. C*** **112, 17726-17736, doi:10.1021/jp8061493 (2008).**

31 Moon, J. S., Lee, J. K., Cho, S. N., Byun, J. Y. & Heeger, A. J. "Columnlike" Structure of the Cross-Sectional Morphology of Bulk Heterojunction Materials. ***Nano Lett.*** **9, 230-234, doi:10.1021/nl802821h (2009).**

32 Muller, C. *et al.* Binary organic photovoltaic blends: A simple rationale for optimum compositions. *Advanced Materials* 20, 3510-+, doi:10.1002/adma.200800963 (2008).

33 Zhao, J. *et al.* Phase Diagram of P3HT/PCBM Blends and Its Implication for the Stability of Morphology. *J. Phys. Chem. B* 113, 1587-1591, doi:10.1021/jp804151a (2009).

34 Carter, D. B. W. C. B. *Transmission Electron Microscopy*. 2 edn, (Springer, 1996).

35 Germack, D. S. *et al.* Substrate-dependent interface composition and charge transport in films for organic photovoltaics. *Appl. Phys. Lett.* 94, doi:233303 10.1063/1.3149706 (2009).

36 Xu, Z. *et al.* Vertical Phase Separation in Poly(3-hexylthiophene): Fullerene Derivative Blends and its Advantage for Inverted Structure Solar Cells. *Advanced Functional Materials* 19, 1227-1234, doi:10.1002/adfm.200801286 (2009).

37 van Bavel, S. S., Barenklau, M., de With, G., Hoppe, H. & Loos, J. P3HT/PCBM Bulk Heterojunction Solar Cells: Impact of Blend Composition and 3D Morphology on Device Performance. *Advanced Functional Materials* 20, 1458-1463, doi:10.1002/adfm.200902247 (2010).

38 Egerton, R. F. *Electron Energy-Loss Spectroscopy in the Electron Microscope*. 2 edn, (Plenum Press, 1986).

39 Diebold, A. C. *Handbook of Silicon Semiconductor Metrology*. (Marcel Dekker Inc., 2001).

40 Treat, N. D. *et al.* Interdiffusion of PCBM and P3HT Reveals Miscibility in a Photovoltaically Active Blend. *Advanced Energy Materials* 1, 82-89, doi:10.1002/aenm.201000023 (2011).

41 Wang, X. *et al.* High-Resolution Spectroscopic Mapping of the Chemical Contrast from Nanometer Domains in P3HT:PCBM Organic Blend Films for Solar-Cell Applications. *Advanced Functional Materials* 20, 492-499, doi:10.1002/adfm.200901930 (2010).

42 van Bavel, S. S., Bärenklau, M., de With, G., Hoppe, H. & Loos, J. P3HT/PCBM Bulk Heterojunction Solar Cells: Impact of Blend Composition and 3D Morphology on Device Performance. *Advanced Functional Materials* 20, 1458-1463 (2010).

43 Guan, Z. L. *et al.* Direct determination of the electronic structure of the poly(3-hexylthiophene):phenyl-[6,6]-C61 butyric acid methyl ester blend. *Organic Electronics* 11, 1779-1785, doi:10.1016/j.orgel.2010.07.023 (2010).

44 Gao, Y. Q., Martin, T. P., Thomas, A. K. & Grey, J. K. Resonance Raman Spectroscopic- and Photocurrent Imaging of Polythiophene/Fullerene Solar Cells. *J. Phys. Chem. Lett.* 1, 178-182, doi:10.1021/jz900038c (2010).

45 Chiu, M. Y., Jeng, U. S., Su, M. S. & Wei, K. H. Morphologies of Self-Organizing Regioregular Conjugated Polymer/Fullerene Aggregates in Thin Film Solar Cells. *Macromolecules* 43, 428-432, doi:10.1021/ma901895d (2010).

46 Jimison, L. H., Toney, M. F., McCulloch, I., Heeney, M. & Salleo, A. Charge-Transport Anisotropy Due to Grain Boundaries in Directionally Crystallized Thin Films of Regioregular Poly(3-hexylthiophene). *Advanced Materials* 21, 1568-1572, doi:10.1002/adma.200802722 (2009).

47 Chen, H.-Y. *et al.* Fast-Grown Interpenetrating Network in Poly(3-hexylthiophene): Methanofullerenes Solar Cells Processed with Additive. *The Journal of Physical Chemistry C* 113, 7946-7953, doi:doi:10.1021/jp810798z (2009).

48 **Brinkmann, M. & Rannou, P. Molecular Weight Dependence of Chain Packing and Semicrystalline Structure in Oriented Films of Regioregular Poly(3-hexylthiophene) Revealed by High-Resolution Transmission Electron Microscopy. *Macromolecules* 42, 1125-1130, doi:10.1021/ma8023415 (2009).**

49 **Germack, D. S. *et al.* Substrate-dependent interface composition and charge transport in films for organic photovoltaics. *Applied Physics Letters* 94, 233303 (2009).**

50 **Guan, Z. L. *et al.* Direct determination of the electronic structure of the poly(3-hexylthiophene):phenyl- 6,6 -C61 butyric acid methyl ester blend. *Organic Electronics* 11, 1779-1785, doi:10.1016/j.orgel.2010.07.023 (2010).**

51 **Renaud, G., Lazzari, R. & Leroy, F. Probing surface and interface morphology with Grazing Incidence Small Angle X-Ray Scattering. *Surface Science Reports* 64, 255-380, doi:10.1016/j.surfrep.2009.07.002 (2009).**

52 **Baker, J. L. *et al.* Quantification of Thin Film Crystallographic Orientation Using X-ray Diffraction with an Area Detector. *Langmuir* 26, 9146-9151, doi:10.1021/la904840q (2010).**

53 **Li, G. *et al.* "Solvent annealing" effect in polymer solar cells based on poly(3-hexylthiophene) and methanofullerenes. *Advanced Functional Materials* 17, 1636-1644, doi:10.1002/adfm.200600624 (2007).**

54 **Khanna, V. *et al.* Effect of chain architecture and surface energies on the ordering behavior of lamellar and cylinder forming block copolymers. *Macromolecules* 39, 9346-9356, doi:10.1021/ma0609228 (2006).**

55 **Zhou, N., Bates, F. S. & Lodge, T. P. Mesoporous membrane templated by a polymeric bicontinuous microemulsion. *Nano Lett.* 6, 2354-2357, doi:10.1021/nl061765t (2006).**

56 **Teubner, M. & Strey, R. Origin of the scattering peak in microemulsions. *J. Chem. Phys.* 87, 3195-3200 (1987).**

57 **Morkved, T. L., Stepanek, P., Krishnan, K., Bates, F. S. & Lodge, T. P. Static and dynamic scattering from ternary polymer blends: Bicontinuous microemulsions, Lifshitz lines, and amphiphilicity. *The Journal of Chemical Physics* 114, 7247, doi:10.1063/1.1357800 (2001).**

58 **Ruegg, M. L., Reynolds, B. J., Lin, M. Y., Lohse, D. J. & Balsara, N. P. Microphase and macrophase separation in multicomponent A/B/A-C polymer blends with attractive and repulsive interactions. *Macromolecules* 39, 1125-1134, doi:10.1021/ma0516889 (2006).**

59 **Strobl, G. *The Physics of Polymers*. 3 edn, (Springer, 2007).**

60 **Leitao, H., da Gama, M. M. T. & Strey, R. Scaling of the interfacial tension of microemulsions: A Landau theory approach. *J. Chem. Phys.* 108, 4189-4198 (1998).**

61 **Schubert, K. V., Strey, R., Kline, S. R. & Kaler, E. W. SMALL-ANGLE NEUTRON-SCATTERING NEAR LIFSHITZ LINES - TRANSITION FROM WEAKLY STRUCTURED MIXTURES TO MICROEMULSIONS. *J. Chem. Phys.* 101, 5343-5355 (1994).**

62 **Flory, P. J. *Principles of Polymer Chemistry*. 11 edn, (Cornell University Press, 1953).**

63 **Prosa, T. J., Winokur, M. J., Moulton, J., Smith, P. & Heeger, A. J. X-Ray structural studies of poly(3-alkylthiophenes) - an example of an inverse comb. *Macromolecules* 25, 4364-4372 (1992).**

64 **Bulle-Lieuwma, C. W. T. *et al.* Characterization of polymer solar cells by TOF-SIMS depth profiling. *Appl. Surf. Sci.* 203, 547-550 (2003).**

65 **Dennler, G., Scharber, M. C. & Brabec, C. J. Polymer-Fullerene Bulk-Heterojunction Solar Cells. *Advanced Materials* 21, 1323-1338, doi:10.1002/adma.200801283 (2009).**

66 **Chu, C. W. *et al.* Control of the nanoscale crystallinity and phase separation in polymer solar cells. *Applied Physics Letters* 92, 103306, doi:Artn 103306 Doi 10.1063/1.2891884 (2008).**

67 **Park, S. H. *et al.* Bulk heterojunction solar cells with internal quantum efficiency approaching 100%. *Nat. Photonics* 3, 297-U295, doi:10.1038/nphoton.2009.69 (2009).**

68 **Mayer, A. C. *et al.* Bimolecular Crystals of Fullerenes in Conjugated Polymers and the Implications of Molecular Mixing for Solar Cells. *Advanced Functional Materials* 19, 1173-1179, doi:10.1002/adfm.200801684 (2009).**

69 **Parmer, J. E. *et al.* Organic bulk heterojunction solar cells using poly(2,5-bis(3-tetradecyllthiophen-2-yl)thieno 3,2,-b thiophene). *Appl. Phys. Lett.* 92, doi:113309 10.1063/1.2899996 (2008).**

70 **Miller, N. C. *et al.* The Phase Behavior of a Polymer-Fullerene Bulk Heterojunction System that Contains Bimolecular Crystals. *J. Polym. Sci. Pt. B-Polym. Phys.* 49, 499-503, doi:10.1002/polb.22214 (2011).**

71 **Chen, D. A., Nakahara, A., Wei, D. G., Nordlund, D. & Russell, T. P. P3HT/PCBM Bulk Heterojunction Organic Photovoltaics: Correlating Efficiency and Morphology. *Nano Lett.* 11, 561-567, doi:10.1021/nl103482n (2011).**

72 **Moon, J. S., Takacs, C. J., Sun, Y. M. & Heeger, A. J. Spontaneous Formation of Bulk Heterojunction Nanostructures: Multiple Routes to Equivalent Morphologies. *Nano Lett.* 11, 1036-1039, doi:10.1021/nl200056p (2011).**

73 **Kim, S. & Minor, A. FIB preparation of cross-sectional polymer thin film TEM samples. *Microscopy and Microanalysis* 14, 996-997, doi:doi:10.1017/S1431927608085838 (2008).**

74 **Welz, S., Browning, N. & Minor, A. M. Shadow FIBing- Using Geometry to Prepare TEM Samples. *Microscopy and Microanalysis* 11, 834-835, doi:doi:10.1017/S1431927605504872 (2005).**

75 **Kozma, E., Kotowski, D., Bertini, F., Luzzati, S. & Catellani, M. Synthesis of donor-acceptor poly(perylene diimide-altoligothiophene) copolymers as n-type materials for polymeric solar cells. *Polymer* 51, 2264-2270, doi:10.1016/j.polymer.2010.03.040 (2010).**

76 **Sommer, M., Lindner, S. M. & Thelakkat, M. Microphase-separated donor-acceptor diblock copolymers: Influence of HOMO energy levels and morphology on polymer solar cells. *Advanced Functional Materials* 17, 1493-1500, doi:10.1002/adfm.200600634 (2007).**

77 **Zhang, Q., Cirpan, A., Russell, T. P. & Emrick, T. Donor−Acceptor Poly(thiophene-block-perylene diimide) Copolymers: Synthesis and Solar Cell Fabrication. *Macromolecules* 42, 1079-1082, doi:10.1021/ma801504e (2009).**

78 **Sommer, M., Huettner, S. & Thelakkat, M. in *Complex Macromolecular Systems Ii* Vol. 228 *Advances in Polymer Science* 123-153 (Springer-Verlag Berlin, 2010).**

79 **Amundson, K., Helfand, E., Quan, X. & Smith, S. D. Alignment of lamellar block copolymer microstructure in an electric field. 1. Alignment kinetics. *Macromolecules* 26, 2698-2703, doi:10.1021/ma00063a010 (1993).**

80 **Onuki, A. & Fukuda, J.-i. Electric Field Effects and Form Birefringence in Diblock Copolymers. *Macromolecules* 28, 8788-8795, doi:10.1021/ma00130a011 (1995).**

81 **Thurn-Albrecht, T., DeRouchey, J., Russell, T. P. & Jaeger, H. M. Overcoming interfacial interactions with electric fields. *Macromolecules* 33, 3250-3253 (2000).**

82 **Thurn-Albrecht, T. *et al.* Ultrahigh-density nanowire arrays grown in self-assembled diblock copolymer templates. *Science* 290, 2126-2129 (2000).**

83 **Albalak, R. J. & Thomas, E. L. ROLL-CASTING OF BLOCK-COPOLYMERS AND OF BLOCK COPOLYMER-HOMOPOLYMER BLENDS. *J. Polym. Sci. Pt. B-Polym. Phys.* 32, 341-350 (1994).**

84 **Huang, E., Rockford, L., Russell, T. P. & Hawker, C. J. Nanodomain control in copolymer thin films. *Nature* 395, 757-758 (1998).**

85 **Keller, A., Pedemont.E & Willmout.Fm. MACRO-LATTICE FROM SEGREGATED AMORPHOUS PHASES OF A 3 BLOCK COPOLYMER. *Nature* 225, 538-& (1970).**

86 **Majewski, P. W., Gopinadhan, M., Jang, W. S., Lutkenhaus, J. L. & Osuji, C. O. Anisotropic Ionic Conductivity in Block Copolymer Membranes by Magnetic Field Alignment. *Journal of the American Chemical Society* 132, 17516-17522, doi:10.1021/ja107309p (2010).**

87 **Debye, P. & Kleboth, K. ELECTRICAL FIELD EFFECT ON CRITICAL OPALESCENCE. *J. Chem. Phys.* 42, 3155-& (1965).**

88 **Khaliq, A., Xue, F. L. & Varahramyan, K. Numerical simulation of spin coated P3HT organic thin film transistors with field dependent mobility and distributed contact resistance. *Microelectronic Engineering* 86, 2312-2315, doi:10.1016/j.mee.2009.04.009 (2009).**

89 **Szmytkowski, J. Modeling the electrical characteristics of P3HT:PCBM bulk heterojunction solar cells: Implementing the interface recombination. *Semicond. Sci. Technol.* 25, doi:015009 10.1088/0268-1242/25/1/015009 (2010).**

90 **Blom, P. W. M., Mihailetchi, V. D., Koster, L. J. A. & Markov, D. E. Device Physics of Polymer:Fullerene Bulk Heterojunction Solar Cells. *Advanced Materials* 19, 1551-1566, doi:10.1002/adma.200601093 (2007).**